PRIMARY RESEARCH ARTICLE





Variability of sun-induced chlorophyll fluorescence according to stand age-related processes in a managed loblolly pine forest

Roberto Colombo¹ | Marco Celesti¹ | Remo Bianchi² | Petya K. E. Campbell³ | Sergio Cogliati¹ | Bruce D. Cook⁴ | Lawrence A. Corp⁵ | Alexander Damm^{6,7} | Jean-Christophe Domec^{8,9} | Luis Guanter¹⁰ | Tommaso Julitta¹ | Elizabeth M. Middleton⁴ | Asko Noormets¹¹ | Cinzia Panigada¹ | Francisco Pinto^{12,13} | Uwe Rascher¹² | Micol Rossini¹ | Anke Schickling¹²

Correspondence

Roberto Colombo, Remote Sensing of Environmental Dynamics Laboratory, DISAT,

Abstract

Leaf fluorescence can be used to track plant development and stress, and is considered the most direct measurement of photosynthetic activity available from remote sensing techniques. Red and far-red sun-induced chlorophyll fluorescence (SIF) maps were generated from high spatial resolution images collected with the HyPlant airborne spectrometer over even-aged loblolly pine plantations in North Carolina (United States). Canopy fluorescence yield (i.e., the fluorescence flux normalized by the light absorbed) in the red and far-red peaks was computed. This quantifies the fluorescence emission efficiencies that are more directly linked to canopy function compared to SIF radiances. Fluorescence fluxes and yields were investigated in relation to tree age to infer new insights on the potential of those measurements in better describing ecosystem processes. The results showed that red fluorescence yield varies with stand age. Young stands exhibited a nearly twofold higher red fluorescence yield than mature forest plantations, while the far-red fluorescence yield remained constant. We interpreted this finding in a context of photosynthetic stomatal limitation in aging loblolly pine stands. Current and future satellite missions provide global datasets of SIF at coarse spatial resolution, resulting in intrapixel mixture effects, which could be a confounding factor for fluorescence signal interpretation. To mitigate this effect, we propose a surrogate of the fluorescence yield, namely the Canopy Cover Fluorescence Index (CCFI) that accounts for the spatial variability in canopy structure by exploiting the vegetation fractional cover. It was found that spatial aggregation tended to mask the effective relationships, while the CCFI was still able to maintain this link. This study is a first attempt in interpreting the fluorescence variability in aging forest stands and it may open new perspectives in understanding long-term forest dynamics in response to future climatic conditions from remote sensing of SIF.

KEYWORDS

FLEX mission, fluorescence normalization, forest stand age, HyPlant spectrometer, loblolly pine, Parker Tract forest, red fluorescence yield, sun-induced chlorophyll fluorescence

¹Remote Sensing of Environmental Dynamics Laboratory, DISAT, University of Milano-Bicocca, Milan, Italy

²ESA-ESRIN Earth Observations, Frascati, Italy

³Joint Center for Earth Systems Technology, University of Maryland Baltimore County, Baltimore, MD, USA

⁴Biospheric Sciences Laboratory, NASA/ GSFC, Greenbelt, MD, USA

⁵Science Systems & Applications Inc., Lanham, MD, USA

⁶Remote Sensing Laboratories, University of Zurich, Zurich, Switzerland

⁷Department of Surface Waters - Research and Management, Eawag, Swiss Federal Institute of Aquatic Science and Technology, Dübendorf, Switzerland

⁸Bordeaux Sciences Agro, UMR 1391 INRA-ISPA, Gradignan Cedex, France

⁹Nicholas School of the Environment, Duke University, Durham, NC, USA

¹⁰Helmholtz Centre Potsdam, German Research Center for Geosciences (GFZ), Potsdam, Germany

¹¹Department of Forestry & Environmental Resources, North Carolina State University, Raleigh, NC, USA

 $^{^{\}rm 12} Institute$ of Bio and Geosciences, IBG-2: Plant Sciences, Forschungszentrum Jülich GmbH, Jülich, Germany

¹³Global Wheat Program, International Maize and Wheat Improvement Center (CIMMYT), Mexico City, Mexico

University of Milano-Bicocca, Milan, Italy. Email: roberto.colombo@unimib.it

Funding information

ESA/NASA Joint FLEX-US campaign; German Research Foundation (DFG); Duke Provost's Collaboratories initiative, and from the National Science foundation, Grant/ Award Number: NSF-IOS-1754893

1 | INTRODUCTION

Leaf structure and physiology change in many woody species when they become sexually mature (e.g., Greenwood, 1995). Compared with the knowledge of senescence processes in annuals and biennial plants, relatively little is known about age-related changes in woody perennials (Bond, 2000). Old trees differ from younger trees, both physiologically and morphologically. In general, older trees have lower rates of photosynthesis, reduced growth rates (both height and diameter) and a distinctive hydraulic architecture (Meinzer, Lachenbruch, & Dawson, 2011; Ryan & Yoder, 1997). Nutrition, carbon allocation (including respiration), meristematic activity and the tree's hydraulic properties all potentially change with tree age and in most cases result in a slower growth in older trees (Domec & Gartner, 2003). Moreover, it is generally known that photosynthetic rates of seedlings are higher than in mature trees (Larcher, 1969). Leaf photosynthesis and stand primary production have often been found to decline with increasing plant age and size, as a result of hydraulic or biochemical limitations (Drake, Davis, Raetz, & Delucia, 2011; Hubbard, Yoder, & Ryan, 1999; Ryan, Phillips, & Bond, 2006; Yoder, Ryan, Waring, Schoettle, & Kaufmann, 1994). Determining why growth is reduced in aging forest stands is a compelling need: the growth patterns are pronounced and predictable but the underlying mechanisms remain unclear (Gower, McMurtrie, & Murty, 1996; Ryan, Binkley, & Fownes, 1996). Even though some work has been done at the leaf level (de Beeck et al., 2010; Linkosalo, Heikkinen, Pulkkinen, & Mäkipää, 2014; Reinhardt, Johnson, & Smith, 2009; Shirke, 2001), the response of sun-induced chlorophyll fluorescence (SIF) to these age-related processes has not been investigated previously. SIF is closely related to actual photosynthetic rates and basically to the functional process linked to the amount of energy (in form of transported electrons) that is provided from photosynthetic light reactions (Porcar-Castell et al., 2014).

Remote sensing of SIF is a research field of growing interest with the potential to provide an improved tool for monitoring plant status and photosynthetic function from above. In this framework, the new satellite mission of the European Space Agency, the FLuorescence EXplorer (FLEX; Drusch et al., 2017), is expected to map canopy fluorescence from space at global level, with 300 m spatial resolution, which will be used to derive the photosynthetic activity of natural and managed ecosystems. Fluorescence is considered the most direct proxy of actual photosynthetic activity available from remote sensing techniques and as such it has been used extensively to track plant status at leaf and canopy level (Ac et al., 2015; Cheng et al., 2013; Damm

et al., 2010; Daumard et al., 2010; Goulas et al., 2017; Joiner et al., 2014; Koffi, Rayner, Norton, Frankenberg, & Scholze, 2015; Meroni & Colombo, 2006; Meroni et al., 2008; Middleton, Huemmrich, Cheng, & Margolis, 2012; Moya et al., 2004; Rascher et al., 2009; Rossini et al., 2010, 2015; Zarco-Tejada, González-Dugo, & Berni, 2012; Zarco-Tejada, González-Dugo, & Fereres, 2016; Zhang et al., 2014).

The intensity of the fluorescence signal at canopy level depends on the photosynthetic rates, biophysical, biochemical and structural characteristics of the canopy, incoming radiation and background contributions (Cerovic et al., 1996; Damm, Guanter, Paul-Limoges et al., 2015; Damm, Guanter, Verhoef et al., 2015; Daumard et al., 2010; Fournier et al., 2012; Hoge, Swift, & Yungel, 1983; Moya, Daumard, Moise, Ounis, & Goulas, 2006; Olioso, Méthy, & Lacaze, 1992; Rossini et al., 2016; Van Wittenberghe et al., 2013; Verrelst et al., 2015). These parameters are highly variable in space and time and they should all be considered to correctly interpret the fluorescence signal. In fact, plants with different photosynthetic rates, chlorophyll content, and/or canopy structure, and exposed to various irradiance regimes can potentially emit the same amount of fluorescence. The effects of variable incoming illumination can be corrected by computing the apparent fluorescence yield (i.e., the ratio of the emitted fluorescence flux to the total incoming photosynthetically active radiation (PAR), which is in fact the parameter most commonly exploited for spatial and temporal comparison of fluorescence satellite derived products collected in different light illumination conditions (i.e., different solar zenith angles, e.g., Guanter et al., 2014). However, to move toward the use of SIF for net photosynthesis and plant functioning characterization in a heterogeneous landscape, it is also necessary to account for vegetation structural/biochemical variations. This can be accomplished by exploiting the true canopy fluorescence yield (ε_f ; i.e., the ratio of the emitted fluorescence flux to the absorbed photosynthetically active radiation, APAR), which is a physically based index of efficiency that accurately describes the effects of the absorbed radiation on the SIF signal. The usefulness of fluorescence or the apparent fluorescence yield to track the effects of environmental stressors on plant functioning has been demonstrated in numerous investigations (e.g., Guanter et al., 2014; Meroni et al., 2008), while the performances of the true fluorescence yield computed at airborne or satellite level has been investigated in only two studies (Sun et al., 2015; Wieneke et al., 2016). This is mainly due to the difficulty in accurately estimating APAR, which is challenging.

Current and future satellite missions will provide global datasets of fluorescence at a range of coarse spatial resolutions (e.g., 300 m

to 0.5°), resulting in intrapixel mixture effects, which will be an unavoidable confounding factor for fluorescence signal interpretation. In this context, there is a need of having simplified fluorescence indices for small-scale applications over large regions, which can take into account the spatial variability of canopy structure. Therefore, a new approach is needed to compensate for structural effects on SIF measurements, including the use of radiative transfer model inversion (Hernández-Clemente, North, Hornero, & Zarco-Tejada, 2017; van der Tol et al., 2016; Zhao et al., 2016), spectrally invariant correction factors (e.g., the directional area scattering factor, Knyazikhin et al., 2012), or empirical normalization techniques (Colombo, Meroni, & Rossini, 2016).

In this paper, red and far-red SIF maps were generated from high spatial resolution images (1 m) collected with the HyPlant airborne sensor over a range of even-aged stands in loblolly pine forest plantations in North Carolina (United States). The true canopy fluorescence yields for both red and far-red SIF were then computed and investigated with the main aim to understand if fluorescence varies across stands of different ages, according structural and physiological parameters. In this context, we hypothesized that hydraulic limitation in older pines could reflect in a lower fluorescence emission compared to the younger trees, due to the reduced rates of photosynthesis. We were also interested in evaluating the effect of pixel size and the mixture effects on the relationships between fluorescence and stand age. This study can be considered a first attempt in interpreting the fluorescence variability in aging forest stands and it may open new perspectives in understanding long-term forest dynamics from remote sensing of SIF.

2 | DATA AND METHODS

2.1 Study area

This study was performed at the Parker Tract forest in the lower coastal plain near Plymouth, North Carolina, United States, in the context of the joint 2013 ESA/NASA FLEX airborne campaign (Middleton et al., 2017). The forest is a 4,400 ha managed plantation that contains various loblolly pine (Pinus taeda L.) stands of different ages. Parker Tract is a pine forest where stand density is reduced under a prescribed thinning regime as age increases to maximize timber production. According to the Parker Tract forest management plan, pine stand age within the study area ranged from 3 to 46 years old, when the forests have reached high commercial potential and are being harvested. Therefore, we are dealing with juvenile and mature stages. The topography is flat and the climate is maritime temperate zone with a mean annual precipitation of 1320 mm and mean annual temperature of 15.5°C. The Parker Tract forest belongs to the Long-Term Ecological Research Sites and further details on the site are reported in different studies (Domec, Lachenbruch, Pruyn, & Spicer, 2012; Domec, Sun et al., 2012; Noormets et al., 2010). Figure 1 shows the location of the study area and the investigated loblolly pine stands (with their plantation age) overlapped to the HyPlant mosaic of airborne images collected over the investigated forest.

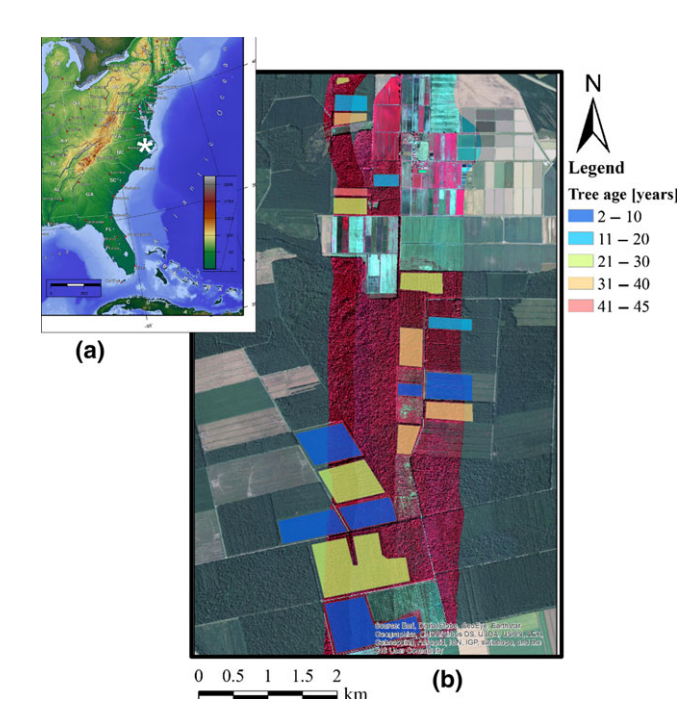


FIGURE 1 (a) Location of the Parker Tract Forest in NC, United States; (b) Location of the loblolly pine even-aged stands (18 total) are shown in colored categories, overlapped on a false color composite *HyPlant* mosaic

The tree age classes reported in Figure 1 correspond to years since planting at the time of data acquisition. In particular, tree ages correspond to the time when the sites were graded and planted with 2-year-old seedlings, and thus can be considered a chronosequence.

Since no direct dendrochronological and only few physiological measurements were available for comparison between forest data and fluorescence estimates, to better interpret our findings we also exploited data and previous results obtained in a companion loblolly forest at the Duke Forest. The Duke Forest loblolly study area is located in the Blackwood Division of Duke Forest (US-Dk3; lat/lon 35.97816586/-79.09419556, North Carolina, USA). It represents a late stage postagricultural succession characteristic of the southeastern United States. Duke Forest, in addition to mixed deciduous forest, also has even-aged plantation of loblolly pine stands ranging from 14 to 114 years, established in 1983 following a clear cut and a burn (Domec et al., 2015; Novick et al., 2009; Oren et al., 2006).

2.2 | Field campaign and leaf-level measurements

During the field survey in September and October 2013, forest stand characteristics including average tree height, crown width, crown depth, and tree diameter at breast height (1.3 m) were measured within one-tenth of an acre (0.4 ha) plots and averaging measurements from two to three plots per stand, at both Parker Tract (18 stands) and Duke Forest (14 stands). Leaf area index (LAI) was measured at all stands using a LAI-2000 Plant Canopy Analyzer (LAI-2000 PCA; Li-Cor, Lincoln, NE, USA). LAI measurements at each

location were taken using a standard protocol in diffuse light conditions within 1 hr of dawn or dusk.

Average carbon (%C) and nitrogen concentration (%N) for pine foliar samples were measured in 26 stands (18 at Duke Forest and 8 at Parker Tract), while leaf chlorophyll content was estimated at 16 stands in Parker Tract. Leaf samples were collected from the two most recent annual leaf flushes on 1-3 branches of the sunlit portion of the upper canopy from three pine trees in a stand, using a cherry picker or a rifle. The branch samples were placed in a bag with wet paper towel, on ice, in a dark cooler and taken to a nearby field laboratory for analysis. Leaf fresh and dry weights were measured on 10 needle fascicles from a sample, using three samples per tree. For pigment determination, needle samples were ground and placed in polystyrene cuvettes containing 4 ml dimethyl sulfoxide (DMSO) and frozen for extraction before the measurements. A spectrophotometer was used to determine chlorophyll a, chlorophyll b, total chlorophyll (Cab, mg/cm²), and carotenoids based on established equations (Chapelle & Kim, 1992).

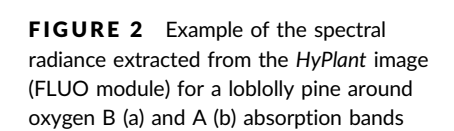
Leaf reflectance and transmittance spectra were also measured on needles collected from 25 trees (1–2 trees per stand at Parker Tract), at the end of the growing season, when the needles were fully developed. Hemispherical reflectance and transmittance were measured using an ASD spectrometer (FieldSpec 3, Analytical Spectral Devices, Inc., Bolder Co.) equipped with an external integrating sphere (LI-1800, Li-Cor, Lincoln, NE, USA) and then used to determine fraction of APAR (fAPAR) at leaf level.

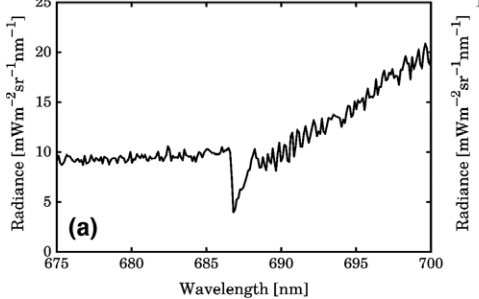
Stomatal conductance (g_s) and net photosynthesis (P_{net}) measurements at the Parker Tract forest were performed in 2013 on May 17, and September 30 for the mature pine trees (23 years old trees) and on June 2 and October 1 for the young trees (7 years old trees). Meteorological conditions were stable during those weeks and were characterized by clear and warm days. Stomatal conductance and photosynthesis were measured with a LI-6400 gas exchange system (LI-COR, Lincoln, NE, USA). Measurements of g_s were performed on six randomly selected individuals within each age class every 2 hr beginning at 06:00 hr solar time and ending at approximately 15:00 hr solar time. Measurements of g_s were conducted on current-year detached fascicles taken from the same shoot simultaneously, and were performed on fully sun exposed south-facing shoots. For the mature trees, shoots from the upper canopy were shot down with a rifle. Needles were not detached for more than 5 min before the measurements were initiated. Previous studies on the same tree species have shown that there were no differences between excised and attached needle gas exchange when measurements were restricted to <15 min after excision (Drake, Raetz, Davis, & Delucia, 2010; Maier, Johnsen, Butnor, Kress, & Anderson, 2002). For each needle, the chamber was set to match prevailing environmental conditions assessed immediately prior to the measurement: atmospheric CO2 concentration (384-405 ppm), relative humidity (46%-61%), photosynthetically active radiation (600–1800 μ mol m⁻² s⁻¹), and leaf temperature (27–35°C). Stomatal conductance and photosynthesis data reported here correspond to the maximum values, i.e., usually taken between 09:30 hr and 11:30 hr solar time. For normalizing g_s on an all-sided leaf area basis, needle areas were obtained geometrically from dimensions measured using a digital caliper (series 500 Mitutoyo, Aurora, IL, USA; Rundel & Yoder, 1998). Along with the gas exchange measurements, leaf water potential (Ψ_{leaf}) were measured at predawn and at midday (11:00 hr-12:00 hr solar time) using a pressure chamber (PMS Ins., Albany, OR, USA). For the midday measurements, Ψ_{leaf} , gs, and Pnet were conducted on detached fascicles taken from the same shoot.

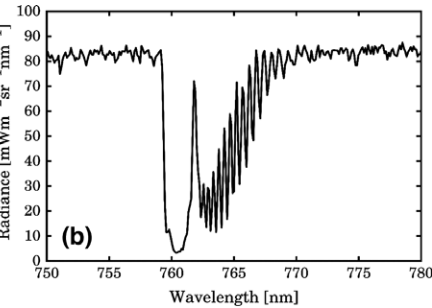
2.3 | Airborne acquisition and preprocessing

On October 26, 2013, from 09:56 hr to 11:08 hr solar time, eight aerial images were acquired by the *HyPlant* airborne imaging spectrometer on board the NASA Langley Research Center's (LARC) UC12 Beechcraft King Air in combination with imagery acquired by the Goddard LiDAR, Hyperspectral and Thermal (G-LiHT) Airborne system. Extensive descriptions of these systems are presented in Rascher et al. (2015), Cook et al. (2013), and Middleton et al. (2017).

The *HyPlant* instantaneous field of view (IFOV) is equal to 0.0832°, while the FOV is of 32.3°. With such a configuration, the aircraft was flown at an average altitude of 610 m, resulting in a *HyPlant* swath of 384 m, with a spatial pixel size of 1 m. *HyPlant* system consists of two modules: the broad band dual-channel module (DUAL) to compute surface reflectance in the visible through near and short wave infrared spectral region (380–2500 nm) and the fluorescence module (FLUO) which operates at higher spectral resolution in the 670–780 nm spectral range designed for fluorescence retrievals. *HyPlant* at-sensor radiance images from the FLUO and the DUAL modules were generated through a dedicated processing chain. The Atmospheric & Topographic Correction model (ATCOR, ReSe Applications Schläpfer) was run to perform the atmospheric correction and then all the images were georectified using the







CaliGeo toolbox (SPECIM, Finland). In addition to reflectance and fluorescence, spectral vegetation indices were generated using the *Hyplant* data. An example of radiance measurements from a loblolly pine acquired with the FLUO module is shown in Figure 2.

A canopy tree height map was obtained from the LiDAR data. Classification of G-LiHT LiDAR ground returns was performed with a progressive morphological filter with Delaunay triangulation to generate a Triangulated Irregular Network (TIN) of ground hits, and the TIN was then used to linearly interpolate the Digital Terrain Model on a 1 m raster grid. Additionally, the TIN was used to interpolate the base elevation of every nonground return, and vegetation heights were computed by difference. The Canopy Height Model (CHM) was created by selecting the greatest return height in every 1 m grid cell. Tree height, defined as the maximum height of each tree, was derived from the CHM by finding the local maximum in a moving window of 3×3 pixels (3×3 m). Local maxima lower than the 1st quartile of the CHM in the stand were not considered representative of a tree, thus they were neglected. The average tree height for each stand was computed as the average of all tree heights (i.e., the local maxima) within each stand.

2.4 Retrieval of sun-induced fluorescence

Among different approaches available for the retrieval of SIF (e.g., Cogliati et al., 2015), the Singular Vector Decomposition (SVD; Guanter et al., 2012, 2013) was selected for this study based on successful results with *Hyplant* data in other studies (e.g., Rossini et al., 2015). This data-driven approach relies on two key assumptions: (i) a given radiance spectrum can be modeled as the linear combination of a reflected surface radiance plus a SIF emission propagated to at-sensor level, and (ii) the reflected surface radiance can be formulated as a linear combination of orthogonal spectral vectors. The SVD is comparable to a principal component analysis and reduces the dimensionality of a large set of correlated variables (e.g., training radiance spectra that are free of SIF emissions) by transforming it into a small set of uncorrelated variables (singular vectors).

The definition of a forward model (*F*) to describe a measured radiance signal including SIF emissions at sensor level comprises several spectral functions (singular vectors) representing the signal intensity due to surface albedo, illumination angle, atmospheric absorption and scattering effects, spectral slope as a function of surface reflectance, and sensor effects (spectral shifts, band broadening). Furthermore, SIF radiance (Wm⁻² sr⁻¹ nm⁻¹) is considered as an additive component to complement the forward model as:

$$F(\omega,\mathsf{SIF}) = \sum\nolimits_{i=1}^{n_{\mathsf{v}}} \omega_i v_i + \mathsf{SIF}, \tag{1}$$

where ω_i corresponds to the weight of a particular singular vector v_i . Typically, 4–5 singular vectors are used to model the at-sensor radiance signal, considering an empirical threshold of 0.05% as minimum information content of a singular vector.

Few adjustments were applied to improve the inversion results, such as removing the strongest absorption features since the forward model does not include any physical formulation of atmospheric absorption or scattering effects, nor the normalization of input radiances and radiances used to obtain the singular vectors based on their spectral slope.

The inversion of F was done by means of standard least squares fitting using a retrieval error covariance S_e that is given as:

$$S_e = \delta_m^2 (J^T J)^{-1}, \tag{2}$$

where δ_m is the measurement error approximated as standard deviation of a subset of used reference radiance signals and J is the matrix containing the singular vectors and J^T is its transpose.

The SVD algorithm was applied to the *HyPlant* FLUO data to produce maps for the canopy red SIF radiances at 690 nm and far-red SIF 740 nm radiances at the full native *HyPlant* spatial resolution (1 m).

2.5 | Retrieval of absorbed photosynthetic active radiation

The APAR maps were computed as the product of fAPAR and the incoming PAR values. fAPAR can be derived from remote sensing, exploiting either physically based or empirical strategies using spectral vegetation indices (e.g., D'Odorico et al., 2014; Donohue, Roderick, & McVicar, 2008; Gobron et al., 2006; Myneni et al., 2002; Pickett-Heaps et al., 2014; Walter-Shea, Privette, Cornell, Mesarch, & Hays, 1997; Widlowski, 2010). Following a scheme analogous to Damm et al. (2010), but using the spectral reflectance instead of the incident and reflected radiance, fAPAR was computed in this study as (1-reflectance) in the PAR region (400–700 nm). In addition, for comparison purposes, we also estimated fAPAR as a linear model of Normalized Difference Vegetation Index (NDVI; Goward & Huemmrich, 1992; Hatfield, Asrar, & Kanemasu, 1984; Liu, Guan, & Liu, 2017; Myneni & Williams, 1994).

The incident PAR was measured at the US-NC2 loblolly plantation flux tower at half-hourly steps, and interpolated to actual overflight times with a piecewise polynomial smoothing spline. During the overpasses (i.e., between 09:56 hr and 11:08 hr solar time), PAR varied between 1,130 μ mol m⁻² s⁻¹ and 1,430 μ mol m⁻² s⁻¹ (247 to 313 W/m²).

2.6 | Computation of true fluorescence yields of loblolly pine

The SIF flux can be modeled as the product of PAR, fAPAR, and ε_f . The last term is the amount of absorbed radiation emitted as fluorescence, and is referred to here as canopy-level "true fluorescence yield" (e.g., Lee et al., 2013):

$$\mathsf{SIF}_{[\lambda,t]} = \varepsilon_{f[\lambda,t]} \cdot \mathsf{PAR}_{[400-700,t]} \cdot \mathsf{fAPAR}_{[t]} \tag{3}$$

The fluorescence flux is dependent on wavelength (λ) and time (t) at which the flux is emitted. For full emission spectra, the entire wavelength range from 650 nm to 800 nm should be considered. Canopy-level true fluorescence yield is related to leaf-level fluorescence yield, neglecting a second-order term accounting for the

reabsorption of the red fluorescence within the canopy and the canopy anisotropy, at both red and far-red wavelengths (Damm, Guanter, Paul-Limoges et al., 2015; Guanter et al., 2014).

In this study, the computation of the SIF yields at full (1 m) spatial resolution was conducted selecting only the loblolly SIF radiance in each stand. A supervised classification scheme based on the HyPlant DUAL reflectance images was therefore implemented to identify loblolly pine (mainly sunlit pixels). Two hundred training pixels were randomly selected and visually assigned to one of the four spectrally distinguishable classes (i.e., loblolly pine, shadow, bare soil, and other vegetation components). The classified map was used as a mask to extract SIF and APAR of the loblolly component within 18 different stands identified as regions of interest (ROI) of 84×84 pixels each. The dimension of the ROI was set according to the forest stand dimensions to get an average stand values of red and farred SIF and APAR for the loblolly component (hereafter SIF lob SIF⁷⁴⁰ and APAR_{lob}), and the corresponding true fluorescence yields (hereafter $\varepsilon_{\rm lob}^{690}$ and $\varepsilon_{\rm lob}^{740}$). The subscript lob indicates the loblolly pine class. The ROIs were selected as close to nadir as possible in order to minimize possible effects dependent on airborne cross-track viewing angles.

The true fluorescence yield maps of the loblolly component were then obtained using Equations 4 and 5, based on values from the maps of loblolly SIF and APAR.

$$\varepsilon_{\text{lob}}^{690} = \frac{\text{SIF}_{\text{lob}}^{690}}{\text{APAR}_{\text{lob}}} \tag{4}$$

$$\varepsilon_{\text{lob}}^{740} = \frac{\text{SIF}_{\text{lob}}^{740}}{\text{APAR}_{\text{lob}}} \tag{5}$$

where $APAR_{lob}$ is the product of PAR and fAPAR maps of the loblolly pine obtained with the different overpasses. We also tested the apparent fluorescent yield, usually employed in remote sensing of fluorescence studies when information about APAR is not available.

2.7 | Spatial aggregation and definition of the Canopy Cover Fluorescence Index

In the analysis at full resolution, the scheme used in this study was similar to that suggested by Zarco-Tejada et al. (2004) and Malenovský et al. (2013), so that the SIF yields were mainly extracted from sunlit pixels. The 1 m pixel size allowed the detection of pixels of homogenous vegetation within the stands. *HyPlant* data were collected in October when the dominant green land cover type was the loblolly pine. Other components, such as understory and deciduous trees, were mainly displaying early autumn senescent foliage, while shadows and bare soils were the most common classes in older and younger stands, respectively. In these forests, when data are aggregated to even 10 m spatial resolution, these components become mixed and it becomes difficult to find and isolate loblolly components.

To evaluate if the relationships between SIF and age-related processes are affected by pixel size (surface heterogeneity), a simple spatial aggregation analysis was carried out by resampling the data at different spatial resolutions (i.e., pixel sizes of 10×10 , 30×30 , 60×60 , and 84×84 pixels). The maximum aggregation was fixed at 84×84 pixels in order to be consistent with the overall stand size, since larger aggregations would result in including trees with different ages. The output of this process generated maps at different pixel (p) sizes, using aggregated red and far-red fluorescence radiances (SIF $_p^{690}$, SIF $_p^{740}$), APAR $_p$, red fluorescence and far-red fluorescence

rescence yields (
$$\varepsilon_p^{690} = \frac{\mathsf{SIF}_p^{690}}{\mathsf{APAR}_n}$$
; $\varepsilon_p^{740} = \frac{\mathsf{SIF}_p^{740}}{\mathsf{APAR}_n}$).

We can reasonably assume that the fluorescence value of a generic pixel p can be expressed with a linear mixing model driven by vegetation fractional cover (ESA, 2017; Hernández-Clemente et al., 2017; Zarco-Tejada, Suarez, & Gonzalez-Dugo, 2013). In this study, the vegetation fractional cover of the loblolly (fclob) was computed as the ratio between the number of pixels of the loblolly class divided by total number of pixels in the ROI. For the case having only two components within a pixel, the fluorescence flux of the aggregated pixel can be derived from the target component (i.e., in this case the loblolly pine SIF, SIF $_{\rm lob}^{690}$, SIF $_{\rm lob}^{740}$), the fluorescence of the other components (oc) within the pixel (SIF $_{\rm oc}^{690}$, SIF $_{\rm oc}^{740}$) and the fractional cover of the loblolly pine. Therefore, the aggregated red SIF radiance can be estimated as follows:

$$SIF_{p}^{690} = SIF_{lob}^{690} \cdot fc_{lob} + SIF_{oc}^{690} \cdot (1 - fc_{lob})$$
 (6)

The SIF_{oc}^{690} term in the study area is mainly a combination of senescent vegetation, bare soil, and shadows, and we can reasonably consider that such fluorescence flux is almost null or negligible. The fluorescence flux of the loblolly component can be therefore directly derived by the knowledge of the aggregated SIF value and its fractional cover. Using this scheme, we can introduce the Canopy Cover Fluorescence Index (CCFI) that makes use of the loblolly cover fraction within the pixel rather than the typically used fAPAR as the basis for normalizing the SIF fluxes:

$$CCFI^{690} = \frac{SIF_p^{690}}{fc_{lob}}$$
 (7)

This index is considered here to be independent from the spatial variability of land cover proportions within each pixel. In other words, for a single vegetation class discontinuously covering the soil surface, the CCFI approximates $\varepsilon_{\rm lob}^{690}$, allowing comparisons of fluorescence across spatial scales without bias due to the different amounts of vegetation coverage in each pixel.

2.8 | Statistical analysis

The previously described fluorescence metrics were investigated across stands of different ages with data aggregated to different spatial resolutions, by using regression models. Statistical analysis and coding was performed in Matlab R2016a (MathWorks, USA) and

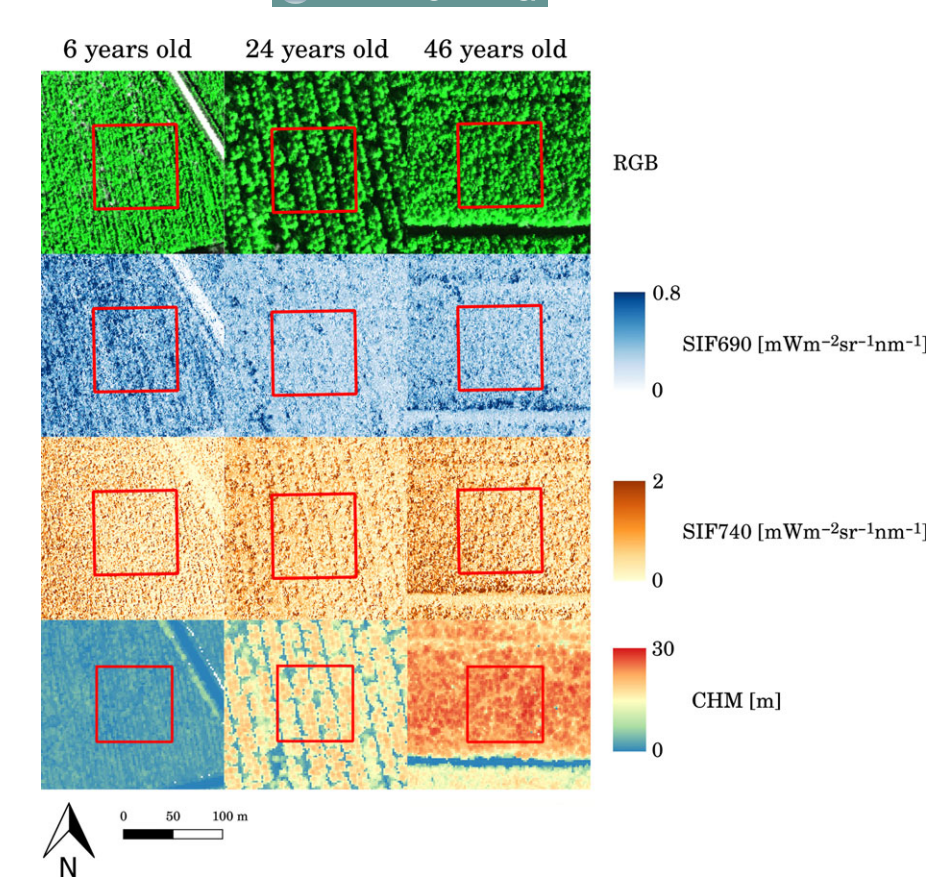


FIGURE 3 Example of three loblolly pine stands characterized by different ages and heights (left to right: 6, 24, and 46 years old). From top to bottom: RGB color composite from the HyPlant DUAL, SIF at 690 nm and 740 nm from the HyPlant FLUO, and canopy height map from the G-LiHT LiDAR. The red squares are the 84×84 pixels regions of interest (ROI) selected for each forest stand

IDL 8.2 (Exelis VIS, USA), while image visualization and rendering was done in ENVI 5.2 (Exelis VIS, USA) and QGIS 2.14 (Quantum GIS Development Team, 2016).

3 | RESULTS

3.1 | Spatial pattern of forest fluorescence

An example of SIF maps for three loblolly pine stands characterized by different ages is shown in Figure 3, with the RGB reflectance map from the *HyPlant* DUAL and the Canopy Height Model derived from the G-LiHT LiDAR data. The different proportions of shadow and sunlit canopy, as well as the spatial arrangement of the sunlit and shadowed components, are clearly distinguishable in the three stands. In particular, in the younger stands, the row-structured pattern followed up for plantation is clear, while in the oldest stand canopy closure obscures the planting arrangement. Fluorescence maps show similar spatial patterns, with lower values in bare or shadowed areas and higher values in the sunlit portion of the canopy. The intercrown gap pattern in the younger stands is clearly visible both in red and far-red SIF maps.

Fluorescence at 690 nm and 740 nm for loblolly pine class ranged between 0.2 and 0.8 mW m $^{-2}$ sr $^{-1}$ nm $^{-1}$ and between 0.3 and 1.2 mW m $^{-2}$ sr $^{-1}$ nm $^{-1}$, respectively. Nonfluorescent targets (e.g., the roads between the stands) showed SIF values close to zero, indicating the reliability of the SIF maps. Overall, the SIF emission magnitude of loblolly pine is relatively low compared to

dense deciduous forests, as reported in previous studies (Rossini et al., 2016) and the values compare well with SIF ground observations obtained over similar loblolly pine stands (ESA, 2015).

3.2 | Reflectance measurements and fAPAR maps

Reflectance and transmittance measurements of loblolly pine needles allowed the computation of the average leaf fAPAR (Figure 4). The proportion of reflected PAR was approximately 8% and the transmitted PAR was ~3%, while the remaining fraction of the total incoming PAR was absorbed (fAPAR = 0.89 or 89%; standard deviation = 0.021). Since at individual leaf level, only

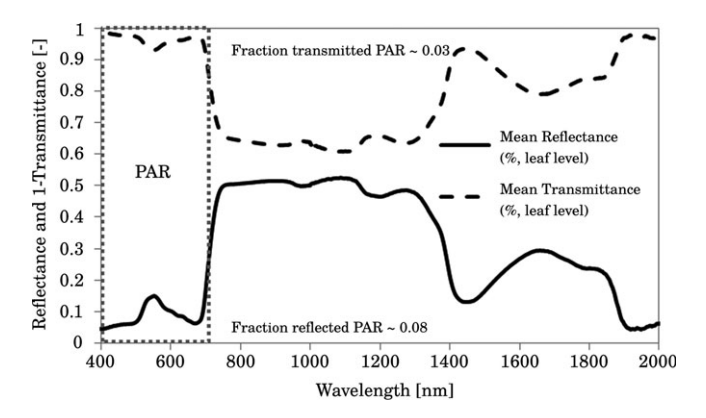


FIGURE 4 Loblolly pine leaf optical properties (mean reflectance and transmittance)

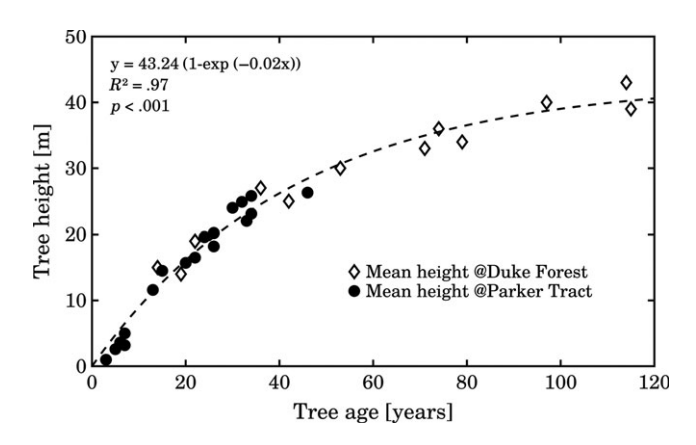


FIGURE 5 Relationship between tree height and age at Parker Tract (closed symbols) and Duke Forest (open symbols, Drake et al., 2010; $R^2 = .97$)

about 3% of PAR is transmitted (but subsequently potentially absorbed by other leaves), we are confident that the approach used in this study to generate fAPAR maps may only slightly overestimate canopy fAPAR, and therefore potentially underestimate fluorescence yield.

The strong correlation between the two estimates of fAPAR ($R^2 = .67$ RMSE = 0.05, p < .001), using the methods previously presented, increases the confidence in our results.

3.3 | Structural, biophysical, biochemical parameters, and leaf gas exchanges

The relationship between tree age and canopy height derived from the G-LiHT LiDAR data at Parker Tract was compared with that measured at the Duke Forest by Drake et al. (2010) for pines. A very

TABLE 1 Coefficient of determination (R^2) and p-value of the linear relationships between stand age (and height) vs. vegetation variables: total chlorophyll content (Cab), Leaf Area Index (LAI), carbon (C), and nitrogen concentration (N)

| Relationships | R ² | p-Value |
|----------------------|----------------|-----------|
| Age (height) vs. Cab | .01 (.01) | .68 (.68) |
| Age (height) vs. LAI | .13 (.13) | .06 (.04) |
| Age (height) vs. C | .05 (.06) | .26 (.22) |
| Age (height) vs. N | .03 (.03) | .42 (.39) |

similar relationship between tree height vs. age was found (Figure 5), suggesting that stands at both forests may belong to the same Site Index and could present similar aging patterns. At the Duke Forest, canopy height ranged from 14 to 43 m, while at the Parker Tract forest tree height varied from 1 to 26 m. Figure 5 shows the relationship between tree age and height for the full dataset including stands from both Parker Tract and Duke Forest modeled using the Gompertz equation (Zeide, 1993).

Table 1 and Figure 6 show the relationships between stand age and height (in brackets) with the biophysical and biochemical parameters measured in field and laboratory. These results clearly show that there were no significant relationships between these variables.

The leaf-level stomatal conductance (g_s ; mean and standard error of six trees) of young trees was found 82.1 (6.4)/58.2 (5.8); (mmol m⁻² s⁻¹) in June/September, respectively, while for mature trees, it was 61.2 (5.7)/49.5 (4.2); (mmol m⁻² s⁻¹) in June/September, respectively. p values for both dates between mature and young trees were <.01. Similarly, leaf-level net photosynthesis (P_{net}) of young and mature trees measured in June were 7.0 (0.5) and 5.8 (0.6) μ mol m⁻² s⁻¹, respectively, and in September were 5.7 (0.7) and 3.8

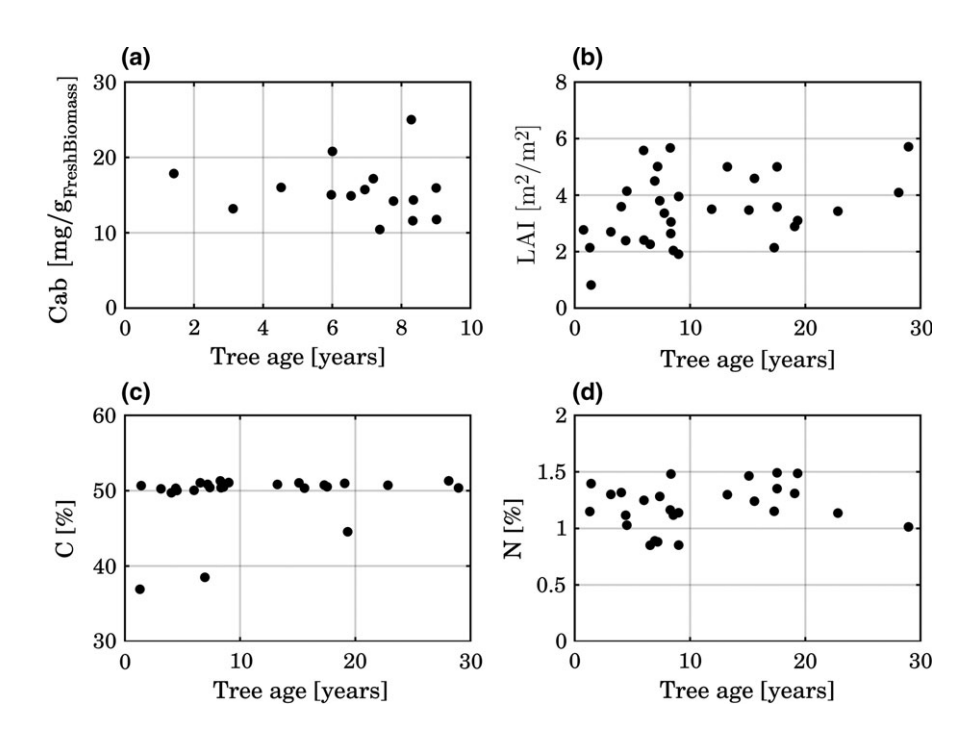


FIGURE 6 Scatter plot between loblolly tree age and total Cab (a), LAI (b), C (c), and N (d)

(0.6) μ mol m⁻² s⁻¹, respectively (p values for both dates for $P_{\rm net}$ between mature and young trees were <.01). Across stand age, the reduction in $P_{\rm net}$ was highly correlated with the decline in $g_{\rm s}$ ($P_{\rm net}=0.089\times g_{\rm s}$; $R^2=.84$; with $g_{\rm s}$ in mmol m⁻² s⁻¹ and $P_{\rm net}$ in μ mol m⁻² s⁻¹). Water stress had a larger effect on $P_{\rm net}$ in old trees than in young trees, even though old trees had similar (p=.42) predawn water potentials in June and even higher (p<.001) ones (less negative) in September than young trees (data not shown). The decline in $P_{\rm net}$ between June and September was indeed 18.6% in young trees and 34.5% in mature trees.

3.4 | Relationship between loblolly fluorescence, APAR, true fluorescence yield, and tree age

The relationship between loblolly fluorescence and tree age obtained at Parker Tract is shown in Figure 7. Loblolly SIF was derived by HyPlant data at full spatial resolution, while stand age was derived from the Parker Tract management plan (n = 18 stands).

Both, SIF_{lob}^{690} and SIF_{lob}^{740} show some variability among stands but only SIF_{lob}^{690} exhibits a statistically significant relationship with tree age. In the case of red fluorescence, a nonlinear decline shows that young forest stands emit slightly more red fluorescence compared to older trees (Figure 7a). Overall, we tested different models and we

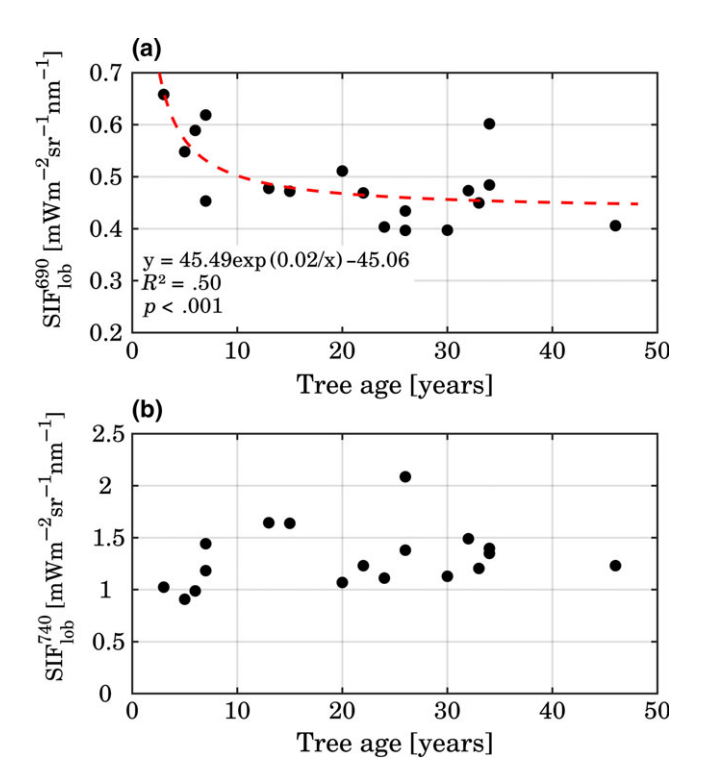


FIGURE 7 Mean SIF radiance values (at 690 nm and 740 nm) for the loblolly component, extracted as the average value of the loblolly class in each ROI, and plotted vs. tree age. The far-red SIF radiance is relatively constant so that the SIF vs. tree age relationship is not statistically significant [Colour figure can be viewed at wileyonlinelibrary.com]

found that the exponential model described the data best, producing the highest coefficient of determination.

Loblolly APAR shows instead a subtle change with age (Figure 8), with younger stands that absorb less PAR radiation than older canopies.

Although there is a link between APAR and SIF, the latter typically shows an additional response to plant physiology and quickly varies with changing photosynthetic activity even before any variation in the pigment pool occurs (e.g., Rossini et al., 2015). Hence, the relationship between SIF and APAR is not univocal, and they provide complementary information on different aspects of the photosynthetic process.

The relationships between the true red SIF yield and tree age is shown in Figure 9. The nonlinear decrease in $\varepsilon_{\rm lob}^{690}$ with age is more pronounced and clearer than for SIF, while there is still no relationship for the far-red SIF yield. True SIF yield performed better than apparent SIF yield which was less related to stand age, with results similar to that found for SIF radiance ($R^2 = .41$, data not shown).

Overall, young stands exhibiting red SIF yield up to 90% higher than older trees (e.g., $3.8 \text{ vs. } 2.2 \text{ sr}^{-1} \text{ nm}^{-1}$).

3.5 | Impact of spatial aggregation on SIF-tree age relationships and performances of the Canopy Cover Fluorescence Index

The relationships between spatially aggregated ($84 \text{ m} \times 84 \text{ m}$) red SIF radiances and true red SIF yield vs. stand age are shown in Figure 10. In this case, aggregated pixels are implicitly composed of mixtures of different components.

Although, it is still possible to observe a slight linear decline of both SIF $_p^{690}$ and ε_p^{690} with age, at this coarser spatial resolution this relationship cannot be easily revealed. Similarly, diminishing success for results (in terms of functional relationship and coefficient of determination) were also found when aggregating at 10 m \times 10 m, 30 m \times 30 m, and 60 m \times 60 m spatial resolutions ($R^2 = .30$; $R^2 = .27$; $R^2 = .25$, respectively). We underscore that aggregated pixels never resulted in mixed stands with different ages. Such analysis is beyond the scope of this study. In addition, no statistically significant relationships were found between either $APAR_p$ and stand age or SIF_p^{740} at different aggregation levels (data not shown).

Figure 11a shows the relationship between the fractional cover of the loblolly pine stands and the spatially aggregated red SIF (84 m \times 84 m) and indicates that fluorescence is fairly affected by this parameter. The SIF signal at this spatial resolution is in fact a mixture of the fluorescence fluxes emitted by tree crowns, both sunlit and shadowed, and understory with different proportion of bare soils and canopy gaps, which causes a variability in the emitted fluorescence flux over stands with different vegetation cover. Moreover, we also tested the relationship between loblolly fractional cover and tree age and we did not find any statistically significant result, although a relevant variability of fractional cover across the different stands (Figure 11b).

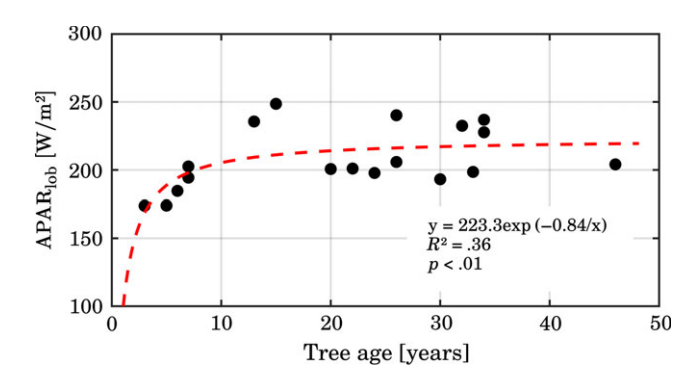


FIGURE 8 Loblolly APAR values vs. tree age for the 18 ROIs [Colour figure can be viewed at wileyonlinelibrary.com]

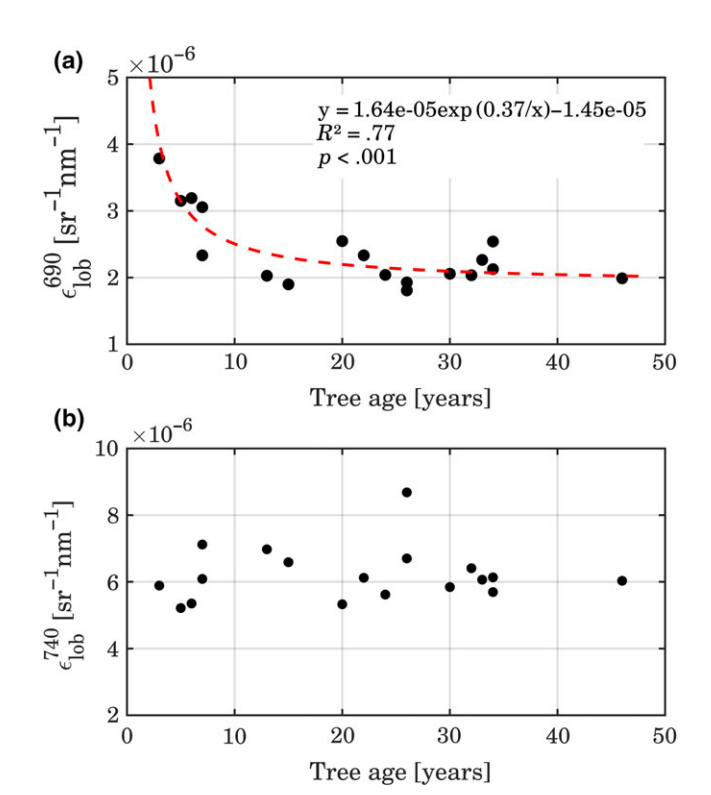


FIGURE 9 Red and far-red SIF yields for loblolly pine vs. tree age for observations acquired at 1 m [Colour figure can be viewed at wileyonlinelibrary.com]

To properly interpret SIF in mixed pixel situations, typical of satellite remote sensing, the spatial variability of vegetation fractional cover has to be taken into account. The relationship between Canopy Cover Fluorescence Index and tree age obtained with aggregated pixel data (84 m \times 84 m) is shown in Figure 12.

Clearly, CCFI is not the same physical quantity as the fluorescence yield, since it is not normalized by APAR. However, it can provide a surrogate of $\varepsilon_{\rm lob}^{690}$ with potential to account for subpixel heterogeneity in coarse spatial resolution data. The relationship shown in Figure 12, closely resembles those for the loblolly red SIF (Figure 7a) and its yield (Figure 9a), providing justification and support for the use of this index in interpreting SIF retrieved from coarse resolution mixed pixels.

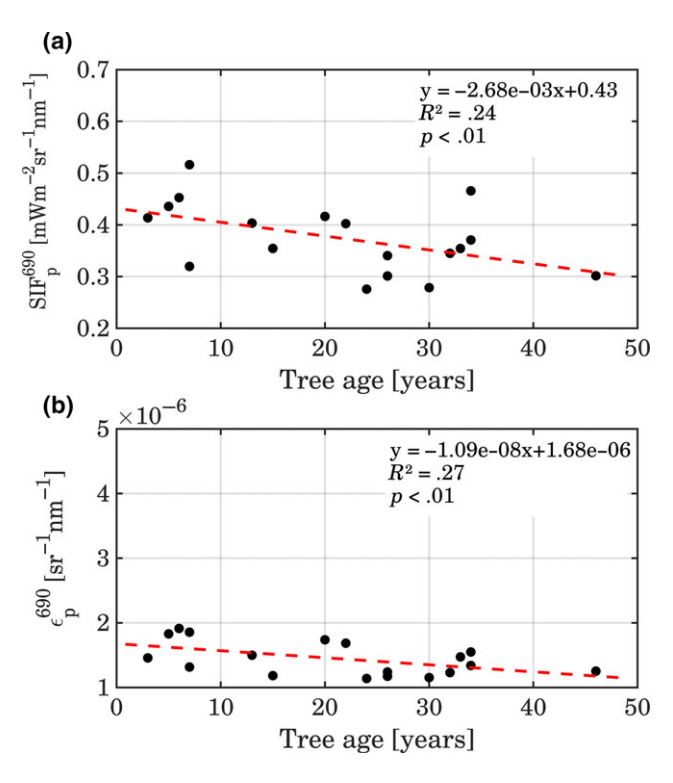


FIGURE 10 Mean of red SIF radiance (upper panel) and the true red SIF yield (lower panel) computed at coarse spatial resolution ($84 \text{ m} \times 84 \text{ m}$) vs. tree age. Note that the axis ranges are deliberatively set equal to those of Figures 7a and 9a, respectively, in order to facilitate visual comparison [Colour figure can be viewed at wileyonlinelibrary.com]

4 | DISCUSSION

4.1 | Sun-induced canopy fluorescence and agerelated processes

A growing body of evidence demonstrates the relationship between fluorescence yields and photosynthetic rates and it is well known that fluorescence can be used to monitor plant stress at leaf and canopy levels (e.g., Ac et al., 2015; Meroni et al., 2009). However, the characteristics of sun-induced canopy fluorescence emissions of forest stands of different age have never been investigated. At treescale, with *HyPlant* data at full spatial resolution, our results clearly indicate that in loblolly pine: (i) red fluorescence and red fluorescence yield change with stand age; measured levels of red SIF were larger in younger trees compared to older ones (up to 60% more SIF $_{\rm lob}^{690}$) and the decline of $\varepsilon_{\rm lob}^{690}$ with stand age (Figure 9a) is more pronounced than that for red SIF (Figure 7a), or for the apparent red fluorescence yield; (ii) onlySIF $_{\rm lob}^{690}$ and $\varepsilon_{\rm lob}^{690}$ declined with tree age, while SIF $_{\rm lob}^{740}$ and $\varepsilon_{\rm lob}^{740}$ did not (Figures 7b and 9b).

Overall, the decline of the true red SIF yield with stand age is more informative than for the apparent red SIF yield (the R^2 value for $\varepsilon_{\rm lob}^{690}$ is about 87% higher than that for the apparent) and more evident than that found for red SIF radiance itself. The use of the true SIF yield is therefore suitable for suppressing, or mitigating, structural variability and canopy pigment absorption and overall, for

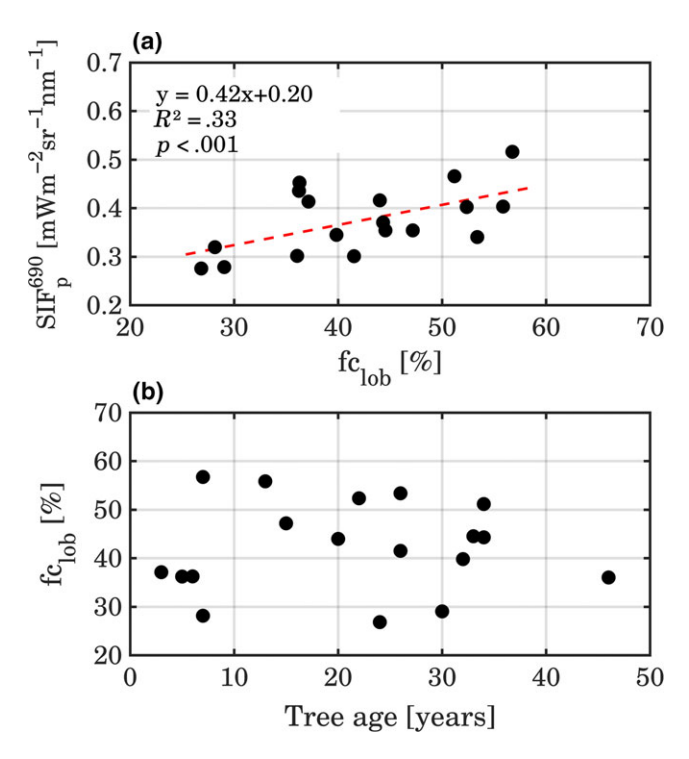


FIGURE 11 Relationships between aggregated (84 m \times 84 m) red fluorescence and loblolly fractional cover (a), and between fractional cover and tree age (b) [Colour figure can be viewed at wileyonlinelibrary.com]

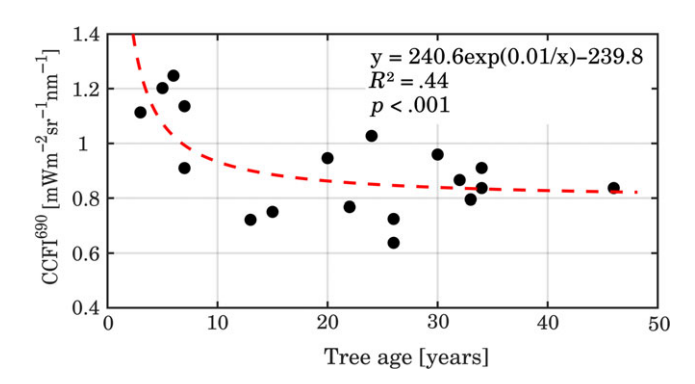


FIGURE 12 CCFI computed for aggregated red SIF vs. tree age [Colour figure can be viewed at wileyonlinelibrary.com]

comparing spatial measurements collected at different times and under different illumination conditions.

No statistically significant relationship was found between LAI, chlorophyll content, and carbon and nitrogen concentration with tree height and age (Table 1 and Figure 6), so that we can reasonably hypothesize that the decline of the red SIF yield with age is not primarily driven by biophysical or biochemical parameters. Consequently, within canopy reabsorption of red SIF radiances should not have a main role in red SIF yield decline related to tree age. The decline of red fluorescence may therefore most likely relate to the underlying physiological processes that downregulate the photosynthetic activity of the plants during their life cycle. Leaf stomatal conductance measurements and net photosynthesis performed at Parker Tract in September clearly show significant reduction with stand age

(7 years old trees = 58.2 mmol m⁻² s⁻¹ for g_s and 5.7 μ mol m⁻² s⁻¹ for P_{net} ; 23 years old trees = 49.5 mmol m⁻² s⁻¹ for g_s and 3.8 μ mol m⁻² s⁻¹ for P_{net}) and potentially explain the drop of red fluorescence with aging. In addition, combining results from predawn water potentials and Pnet we could determine that mature trees had a reduction in 5.5 μ mol m⁻² s⁻¹ MPa⁻¹, as opposed to only $2.9 \mu mol m^{-2} s^{-1} MPa^{-1}$ for the young trees. Those values indicated that between June and September mature trees were more sensitive to soil drying, and that the decline in soil water content had a larger effect on P_{net} in old trees than in young trees. Since these measurements only refer to two stands of young and mature trees, to better interpret our findings we also exploited the results observed in the loblolly pine forest at Duke Forest, which exhibits similar Site Index (Figure 5) and has been used for relevant investigations in this context (Domec, Lachenbruch et al., 2012; Domec, Noormets et al., 2012; Drake et al., 2010, 2011; Noormets et al., 2010). Drake et al. (2010, 2011) showed that light-saturated photosynthetic CO2 uptake, the concentration of CO2 within needle airspaces and stomatal conductance to H2O declined with tree age due to an increasing water limitation of the plants, while stomatal limitation to net photosynthesis increased, supporting the hydraulic limitation hypothesis as revised by Ryan, Binkley, Fownes, Giardina, and Senock (2004) and Ryan et al. (2006). We exploited the stomatal limitation model developed by Drake et al. (2010) and compared it with the observed decline in true red SIF yield, depicting two opposite trends (Figure 13). It is thus plausible to hypothesize that the decline of red SIF yield is a primary consequence of the reduced carbon and water availability induced by the water limitation processes in aging loblolly trees. In other words, the reduced water availability triggers stomata to close, which reduces leaf-internal CO2 concentrations in the leaf tissue and limits the ability of the carbon fixing enzyme RuBisCO to fix CO2. This in turn may cause a tailback into the electron transport and finally this is seen in a variation of SIF (Ac et al., 2015; Damm et al., 2010; Flexas et al., 2002; Rascher et al., 2004; Zarco-Tejada et al., 2016). We can also reasonably assume that the decline in red fluorescence is associated with an enhanced nonphotochemical quenching in older compared to younger trees, as observed in recent studies (Gamon & Bond, 2013). Moreover, the observed drop in red SIF yield occurs around age 10-15, which for loblolly corresponds to the physiological age of demarcation between juvenile and mature wood (Tasissa & Burkhart, 1998). Domec, Lachenbruch et al. (2012) and Domec, Noormets et al. (2012) showed that cambial activity is closely related to stomatal conductance, thus further enforcing the link between the observed SIF decline and the increasing water limitation during the physiological maturation process of loblolly pine.

However, the drop we observed in fluorescence yield is steeper than the increase of stomatal limitation reported at Duke Forest. Our data show in fact a sharp drop in red fluorescence yield before age 10–15 and then a limited change, while at Duke Forest the stomatal limitation clearly increases up to 40 years. Additional studies are therefore needed to fully characterize the link between these trends and to further unravel the role of physiology in driving fluorescence

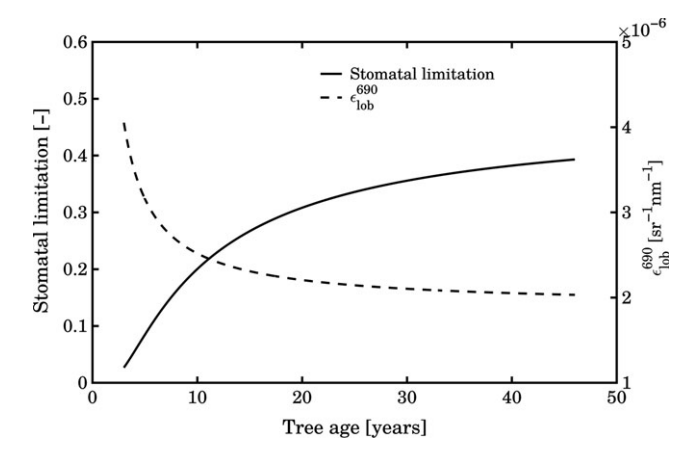


FIGURE 13 Modeled function of the stomatal limitation in the loblolly chronosequence at Duke Forest using the functional forms derived by Drake et al. (2010) and modeled true red SIF yield of the loblolly pine trees at Parker Tract obtained by the function presented in Figure 9a

variability. Even though our analysis has been conducted using pure loblolly pixel only, hence minimizing the effect of canopy closure and mutual shading, the description of the radiative transfer in partly or fully shaded pixels, such as the complex stands in Parker Tract, is challenging and therefore we are aware that other functional and structural factors may partially contribute and explain our findings. Changes in leaf structure, needle length, shoot shape (clumping), and wax deposits on leaf surfaces with aging may in fact alter absorption/ scattering of red fluorescence, enhancing the observed decrease with age. Therefore, we cannot completely discard a residual influence of canopy structure, a generic scattering effect with aging or changes in specific leaf area before and after canopy closure, which is reached at stand age of approximately 10 years. In addition, the complex canopy structure of the older pine trees not only subtly increases the APAR but may also produce stronger reabsorption of the red fluorescence within the canopy and therefore reduce the measured top-of-canopy fluorescence. In this study we have addressed the change in SIF properties from juvenile to mature stands, however future research, considering the natural lifespan of the loblolly trees of 100+ years of age (Burns & Honkala, 1990), is needed to confirm our findings. Moreover, accurate determination of true SIF yield should require an estimation of PAR absorbed by green leaves (e.g., Gitelson & Gamon, 2015; Zhang et al., 2016) and this could be another key point that should be considered for future investigations.

Although a statistically significant decreasing trend is clearly recognizable in the true red SIF yield values as plants become older, no significant relationship with tree age was found with the far-red SIF radiance or yield (Figures 7b and 9b). The fact that red fluorescence, rather than far-red, seems more sensitive to describe these physiological processes can be considered in line with the recent study of Verrelst et al. (2016), which found the red fluorescence as the most sensitive to the canopy net photosynthesis. Unfortunately, only a few recent studies (Cheng et al., 2013; Goulas et al., 2017; Joiner, Yoshida, Guanter, & Middleton, 2016; Louis et al., 2005; Middleton

et al., 2015; Rossini et al., 2015; Wieneke et al., 2016) exploiting both red SIF and far-red SIF have been conducted, and future investigations are necessary to consolidate the results found in this study.

If fluorescence yield changes as trees age, new information will be needed to account for variations in vegetation age classes across landscapes. However, we do not currently know the behavior of fluorescence (or its efficiency) when other species- and age-related processes are involved (e.g., within the hypothesis of nutrient limitation) nor do we know how fluorescence behaves across different ecosystems. Consequently, the relationship between fluorescence and tree age reported here cannot be generalized or used to track age classes. Further studies, especially dedicated experiments and modeling activities, may help in understanding how the fluorescence dynamics can contribute to a better description of the environment, age-related dynamics, and climate interactions. The use of models incorporating fluorescence (e.g., Hernández-Clemente et al., 2017; van der Tol, Verhoef, Timmermans, Verhoef, & Su, 2009) coupled with ecosystem process model for estimating storage and flux of carbon, nitrogen and water (e.g., BIOME-BGC, Running & Gower, 1991) in future research may help in better describing and understanding the role of fluorescence in age-related processes.

4.2 | The need to use normalized SIF metrics at coarse resolution scale

Although new progress has been made in the methodological and technical aspects of fluorescence signal retrieval from space, as shown in recently published global maps (e.g., Joiner et al., 2016), there are definite limitations for SIF interpretation based on large satellite pixels (e.g., GOME-2, 40×80 km; GOSAT, 10×10 km), which are inevitably comprised of mixed components. Although several orbital missions acquire far-red SIF at better spatial resolutions (e.g., OCO-2, 2 × 2 km; and the upcoming ESA TROPOMI/Sentinel-5P, 7×7 km), the possibility to acquire red SIF is not yet available from space at these resolutions. Some of these disadvantages will be mitigated with the advent of the FLEX mission, which will provide complete fluorescence emission spectra globally, including red SIF, at an ecologically relevant spatial scale of 0.3 \times 0.3 km, thus reducing the mixture problems currently encountered. The intrapixel mixture effect is a confounding factor for SIF signal interpretation and it should be mitigated wherever possible. Only after understanding the impact of spatial scale on the SIF signal, it will be possible to properly exploit the use of fluorescence for plant status or for biomass applications in heterogeneous landscapes.

For coarse spatial resolution remote sensing observations, the computation and interpretation of the true fluorescence yield (as presented in Equations 4 and 5) is challenging, due to the challenge in characterization of SIF and APAR for pure target vegetation components. Our results indicate that the mixing of components at coarse spatial resolutions can be considered a "contamination" that hinders the analyses and obscures the relationships between fluorescence and tree age, so that they are no longer clearly detectable in

the aggregated (coarse) pixels. Results from analysis with spatially aggregated data at stand-scale revealed that the relationships between red SIF radiances and yields (Figure 10a,b) were substantially weakened by spatial averaging. In fact, the statistical success in describing the relationship for red SIF vield was reduced by almost 60% ($R^2 = .65 \rightarrow .27$, Figures 9a and 10b) and for red SIF radiances by $\sim 50\%$ ($R^2 = .45 \rightarrow .24$, Figures 7a and 10a), and the aggregated trends appeared more linear, solely due to spatial aggregation from 1 m to 84 m. To mitigate the impact of surface heterogeneity, we propose the CCFI, which was able to produce acceptable results across a range of spatial resolutions (Figure 12). In the use of the CCFI, the fclob normalization may be closely related to the fraction of intercepted PAR (Pickett-Heaps et al., 2014), while less related to the amount of canopy pigments and stand darkness. Thus, CCFI, by exploiting fractional cover, seems able to minimize the effects of canopy structure, enhancing differences in the fluorescence yield of young and old loblolly pine trees.

The vegetation fractional cover is a key vegetation parameter that has already been successfully produced using different remote sensing techniques, by exploiting optical or LiDAR imagery, from several current and past airborne or satellite data operating at different spatial and temporal resolutions (e.g., Baret et al., 2007; Busetto, Meroni, & Colombo, 2008; Carlson & Ripley, 1997; Chen & Cihlar, 1996; Gutman & Ignatov, 1998; Jiménez-Muñoz et al., 2005; Latifovic & Olthof, 2004; North, 2002; Olthof & Fraser, 2007; Verhoef & Bach, 2007). In the context of the FLEX mission, vegetation fractional cover could be dynamically derived at higher spatial resolution from Landsat or Sentinel-2 like missions and then incorporated into the FLEX processing chain to compute the CCFI. The vegetation fractional cover can be more easily estimated than APAR from classification techniques and land use/cover maps. The real benefit in using fractional cover rather than APAR as a normalization tool is that it is more independent of illumination conditions and more stable in time. Thus, it is not mandatory to measure or compute it simultaneously with fluorescence, although it is necessary for APAR, an instantaneous quantity highly dependent on time of acquisition, as fluorescence is. For the satellite perspective, the cosine of the zenith angle normalization can be added to CCFI to take into account the effects of temporal variability of incoming PAR.

The computation of CCFI is quite straightforward since it only requires, in addition to SIF radiances, the knowledge of the fractional vegetation cover in each pixel. However, this normalization cannot be considered as a replacement of the true SIF yield, but rather a complementary index that can be used under specific assumptions. CCFI is not applicable in a general framework at canopy level with airborne or satellite measurements, but only in some conditions, where two components with high fluorescence contrast contribute to the recorded signal. For savannah-like ecosystems, forests without understory and crops in certain phenological phases, this normalization technique may help to better detect plant status and processes. This index is not particularly suited for fragmented agricultural land-scapes with different crops within the same pixel or for complex mixed forests, and therefore additional studies are needed to define strategies for global scale applications. Moreover, further studies

exploiting new emerging 3-D radiative transfer models incorporating fluorescence, like FluorWPS (Zhao et al., 2016), FluorFLIGHT (Hernández-Clemente et al., 2017) and DART (Gastellu-Etchegorry et al., 2017) will help to test the performance of CCFI and the effects caused by the canopy structure on the fluorescence signal recorded from mixed pixels. In summary, the CCFI index can be applied, under certain conditions, to coarse spatial resolution data to minimize confounding factors due to the spatial variability of canopy structure, and it is expected to be suitable for applications assessing vegetation function in future Earth Observations in the fluorescence era.

ACKNOWLEDGEMENTS

This study was supported by ESA/NASA Joint FLEX-US campaign. ESA Contract No. 4000109199/13/NL/FF/lf). Additional support was provided by the Transregional Collaborative Research Centre "Patterns in Soil-Vegetation-Atmosphere-Systems" (TR32/2 2011 3009725), funded by the German Research Foundation (DFG). This research was also supported by a grant from the Duke Provost's Collaboratories initiative, and from the National Science foundation (NSF-IOS-1754893). We gratefully acknowledge Beth Stein and Katie Britt (Dept. of Forest Resources and Environmental Conservation, Virginia Tech, Blacksburg, VA) for supporting field survey and Prof. Federico Magnani (Universitá di Bologna, Italy) and Dott. Franco Miglietta (CNR, Ibimet, Firenze, Italy) for their valuable input. We would like to thank the anonymous Reviewers for the useful comments and suggestions.

ORCID

Roberto Colombo http://orcid.org/0000-0003-3997-0576

REFERENCES

Ac, A., Malenovsky, Z., Olejnickova, J., Gallé, A., Rascher, U., & Mohammed, G. (2015). Meta-analysis assessing potential of steady-state chlorophyll fluorescence for remote sensing detection of plant water, temperature and nitrogen stress. Remote Sensing of Environment, 168, 420–436. https://doi.org/10.1016/j.rse.2015.07.022

Baret, F., Hagolle, O., Geiger, B., Bichero, P., Miras, B., Huc, M., . . . Leroy, M. (2007). LAI, fAPAR and fCover CYCLOPES global products derived from VEGETATION. Part 1: Principles of the algorithm. Remote Sensing of Environment, 110(3), 275–286. https://doi.org/10.1016/j.rse.2007.02.018

Bond, B. (2000). Age-related changes in photosynthesis of woody plants. *Trends in Plant Science*, 5(8), 349–353. https://doi.org/10.1016/S1360-1385(00)01691-5

Burns, R. M., & Honkala, B. H. (1990) Silvics of North America, Vol. 1, Conifers. Washington, DC: U.S.D.A. Forest Service Agriculture Handbook 654.

Busetto, L., Meroni, M., & Colombo, R. (2008). Combining medium and coarse spatial resolution satellite data to improve the estimation of sub-pixel NDVI time series. *Remote Sensing of Environment*, 112(1), 118–131. https://doi.org/10.1016/j.rse.2007.04.004

Carlson, T. N., & Ripley, D. A. (1997). On the relation between NDVI, fractional vegetation cover, and leaf area index. *Remote Sensing of*

- Environment, 62(3), 241–252. https://doi.org/10.1016/S0034-4257 (97)00104-1
- Cerovic, Z. G., Goulas, Y., Gorbunov, M., Briantais, J. M., Camenen, L., & Moya, I. (1996). Fluorosensing of water stress in plants: Diurnal changes of the mean lifetime and yield of chlorophyll fluorescence, measured simultaneously and at distance with a τ-LIDAR and a modified PAM-fluorimeter, in maize, sugar beet, and kalanchoë. *Remote Sensing of Environment*, 58(3), 311–321. https://doi.org/10.1016/S0034-4257(96)00076-4
- Chapelle, E. W., & Kim, M. S. (1992). Ratio analysis of reflectance spectra (RARS): an algorithm for the remote estimation of the concentration of chlorophyll a, Chlorophyll b, and carotenoids in soybean leaves. Remote Sensing of Environment, 39, 239–247. https://doi.org/10.1016/0034-4257(92)90089-3
- Chen, J. M., & Cihlar, J. (1996). Retrieving leaf area index for boreal conifer forests using Landsat TM images. Remote Sensing of Environment, 55, 153–162. https://doi.org/10.1016/0034-4257(95)00195-6
- Cheng, Y. B., Middleton, E. M., Zhang, Q., Huemmrich, K. F., Campbell, P. K., Cook, B. D., ... Daughtry, C. S. (2013). Integrating solar induced fluorescence and the photochemical reflectance index for estimating gross primary production in a cornfield. *Remote Sensing*, 5, 6857–6879. https://doi.org/10.3390/rs5126857
- Cogliati, S., Verhoef, W., Kraft, S., Sabater, N., Alonso, L., Vicent, J., ... Colombo, R. (2015). Retrieval of sun-induced fluorescence using advanced spectral fitting methods. *Remote Sensing of Environment*, 169, 344–357. https://doi.org/10.1016/j.rse.2015.08.022
- Colombo, R., Meroni, M., & Rossini, M. (2016). Development of fluorescence indices to minimize the effects of canopy structural parameters. *Annali di Botanica*, 6, 93–99.
- Cook, B. D., Corp, L. A., Nelson, R. F., Middleton, E. M., Morton, D. C., McCorkel, J. T., ... Montesano, P. M. (2013). NASA Goddard's Lidar, Hyperspectral and Thermal (G-LiHT) airborne imager. *Remote Sensing*, 5, 4045–4066. https://doi.org/10.3390/rs5084045
- Damm, A., Elbers, J., Erler, A., Gioli, B., Hamdi, K., Hutjes, R., . . . Rascher, U. (2010). Remote sensing of sun-induced fluorescence to improve modeling of diurnal courses of gross primary production (GPP). Global Change Biology, 16(1), 171–186. https://doi.org/10.1111/(ISSN)1365-2486
- Damm, A., Guanter, L., Paul-Limoges, E., van der Tol, C., Hueni, A., Buchmann, N., . . . Schaepman, M. E. (2015). Far-red sun-induced chlorophyll fluorescence shows ecosystem-specific relationships to gross primary production: An assessment based on observational and modeling approaches. Remote Sensing of Environment, 166, 91–105. https://doi.org/10.1016/j.rse.2015.06.004
- Damm, A., Guanter, L., Verhoef, W., Schläpfer, D., Garbari, S., & Schaepman, M. E. (2015). Impact of varying irradiance on vegetation indices and chlorophyll fluorescence derived from spectroscopy data. *Remote Sensing of Environment*, 156, 202–215. https://doi.org/10.1016/j.rse. 2014.09.031
- Daumard, F., Champagne, S., Fournier, A., Goulas, Y., Ounis, A., Hanocq, J. F., & Moya, I. (2010). A field platform for continuous measurement of canopy fluorescence. *IEEE Transactions on Geoscience and Remote Sensing*, 48(9), 3358–3368. https://doi.org/10.1109/TGRS.2010. 2046420
- de Beeck, M. O., Gielen, B., Jonckheere, I., Samson, R., Janssens, I. A., & Ceulemans, R. (2010). Needle age-related and seasonal photosynthetic capacity variation is negligible for modelling yearly gas exchange of a sparse temperate Scots pine forest. *Biogeosciences*, 7 (1), 199–215. https://doi.org/10.5194/bg-7-199-2010
- D'Odorico, P., Gonsamo, A., Pinty, B., Gobro, N., Coops, N., Mendez, E., & Schaepman, M. E. (2014). Intercomparison of fraction of absorbed photosynthetically active radiation products derived from satellite data over Europe. Remote Sensing of Environment, 142, 141–154. https://doi.org/10.1016/j.rse.2013.12.005
- Domec, J. C., & Gartner, B. L. (2003). Relationship between growth rates and xylem hydraulic characteristics in young, mature and old-growth

- ponderosa pine trees. *Plant, Cell and Environment*, 26, 471–483. https://doi.org/10.1046/j.1365-3040.2003.00978.x
- Domec, J. C., King, J. S., Ward, E., Oishi, A. C., Palmroth, S., Radecki, A., ... Noormets, A. (2015). Conversion of natural forests to managed forest plantations decreases tree resistance to prolonged droughts. Forest Ecology and Management, 355, 58–71. https://doi.org/10. 1016/i.foreco.2015.04.012
- Domec, J. C., Lachenbruch, B., Pruyn, M., & Spicer, R. (2012). Effects of age-related increases in sapwood area, leaf area, and xylem conductivity on height-related hydraulic costs in two contrasting coniferous species. *Annals of Forest Science*, 69, 17–27. https://doi.org/10.1007/ s13595-011-0154-3
- Domec, J. C., Sun, G., Noormets, A., Gavazzi, M. J., Treasure, E. A., Cohen, E., . . . King, J. S. (2012). A comparison of three methods to estimate evapotranspiration in two contrasting loblolly pine plantations: Age-related changes in water use and drought sensitivity of evapotranspiration components. *Forest Science*, 58(5), 497–512. https://doi.org/10.5849/forsci.11-051
- Donohue, R. J., Roderick, M. L., & McVicar, T. R. (2008). Deriving consistent long-term vegetation information from AVHRR reflectance data using a cover-triangle-based framework. *Remote Sensing of Environment*, 112, 2938–2949. https://doi.org/10.1016/j.rse.2008.02.008
- Drake, J. E., Davis, S. C., Raetz, L. M., & Delucia, E. H. (2011). Mechanisms of age-related changes in forest production: The influence of physiological and successional changes. *Global Change Biology*, 17(4), 1522–1535. https://doi.org/10.1111/j.1365-2486.2010.02342.x
- Drake, J. E., Raetz, L. M., Davis, S. C., & Delucia, E. H. (2010). Hydraulic limitation not declining nitrogen availability causes the age-related photosynthetic decline in loblolly pine (*Pinus taeda* L.): Loblolly pine photosynthesis. *Plant*, *Cell* & *Environment*, 33(10), 1756–1766. https://doi.org/10.1111/j.1365-3040.2010.02180.x
- Drusch, M., Moreno, J., Del Bello, U., Franco, R., Goulas, Y., Huth, A., ... Schuttemeyer, D. (2017). The FLuorescence EXplorer (FLEX) mission concept ESA's Earth Explorer 8. *IEEE TGRS*, 55(3), 1273.
- ESA (2015). FLEX-US Final Report, Technical Assistance for the Deployment of the Airborne HyPlant Imaging Spectrometer during 2013 ESA/NASA Joint FLEX-US (FLuorescence EXplorer Experiment in USA) Campaign. Jülich, Germany: Forschungszentrum.
- ESA (2017). FLEX-EU Final Report, Technical Assistance for the Deployment of an advanced hyperspectral-imaging sensor during FLEX-EU Campaign. Jülich, Germany: Forschungszentrum..
- Flexas, J., Escalona, J. M., Evain, S., Gulías, J., Moya, I., Osmond, C. B., & Medrano, H. (2002). Steady state chlorophyll fluorescence (Fs) measurements as a tool to follow variations of net CO2 assimilation and stomatal conductance during water-stress in C3 plants. *Physiologia Plantarum*, 114(2), 231–240. https://doi.org/10.1034/j.1399-3054. 2002.1140209.x
- Fournier, A., Daumard, F., Champagne, S., Ounis, A., Goulas, Y., & Moya, I. (2012). Effect of canopy structure on sun-induced chlorophyll fluorescence. ISPRS Journal of Photogrammetry and Remote Sensing, 68(1), 112–120. https://doi.org/10.1016/j.isprsjprs.2012.01.003
- Gamon, J. A., & Bond, B. (2013). Effects of irradiance and photosynthetic downregulation on the photochemical reflectance index in Douglasfir and ponderosa pine. *Remote Sensing of Environment*, 135, 141– 149. https://doi.org/10.1016/j.rse.2013.03.032
- Gastellu-Etchegorry, J. P., Lauret, N., Yin, T., Landier, L., Kallel, A., Malenovsky, Z., ... Mitraka, Z. (2017). DART: Recent advances in remote sensing data modelling with atmosphere, polarization, and chlorophyll fluorescence. *IEEE Journal of Selected Topics in Applied Earth Observations and Remote Sensing*, 10(6), 2640–2649. https://doi.org/10.1109/JSTARS.2017.2685528
- Gitelson, A. A., & Gamon, J. A. (2015). The need for a common basis for defining light-use efficiency: Implications for productivity estimation. Remote Sensing of Environment, 156, 196–201. https://doi.org/10. 1016/j.rse.2014.09.017

- Gobron, N., Pinty, B., Taberner, M., Melin, F., Verstraete, M. M., & Widlowski, J. L. (2006). Monitoring the photosynthetic activity of vegetation from remote sensing data. Advances in Space Research, 38, 2196–2202. https://doi.org/10.1016/j.asr.2003.07.079
- Goulas, Y., Fournier, A., Daumard, F., Champagne, S., Ounis, A., Marloie, O., & Moya, I. (2017). Gross primary production of a wheat canopy relates stronger to far red than to red solar-induced chlorophyll fluorescence. *Remote Sensing*, 9(1), 97. https://doi.org/10.3390/rs9010097
- Goward, S. N., & Huemmrich, K. F. (1992). Vegetation canopy PAR absorptance and the normalized difference vegetation index: An assessment using the SAIL model. *Remote sensing of Environment*, 39, 119–140. https://doi.org/10.1016/0034-4257(92)90131-3
- Gower, S. T., McMurtrie, R. E., & Murty, D. (1996). Aboveground net primary production decline with stand age: potential causes. *Trends in Ecology & Evolution*, 11, 378–382. https://doi.org/10.1016/0169-5347(96)10042-2
- Greenwood, M. S. (1995). Juvenility and maturation in conifers: Current concepts. *Tree Physiology*, 15, 433–438. https://doi.org/10.1093/tree phys/15.7-8.433
- Guanter, L., Frankenberg, C., Dudhia, A., Lewis, P. E., Gomez-Dans, J., Kuze, A., & Grainger, R. G. (2012). Retrieval and global assessment of terrestrial chlorophyll fluorescence from GOSAT space measurements. Remote Sensing of Environment, 121, 236–251. https://doi.org/ 10.1016/j.rse.2012.02.006
- Guanter, L., Rossini, M., Colombo, R., Meroni, M., Frankenberg, C., Lee, J. E., & Joiner, J. (2013). Using field spectroscopy to assess the potential of statistical approaches for the retrieval of sun-induced chlorophyll fluorescence from ground and space. Remote Sensing of Environment, 133, 52–61. https://doi.org/10.1016/j.rse.2013.01.017
- Guanter, L., Zhang, Y., Jung, M., Joiner, J., Voigt, M., Berry, J. A., . . . Griffis, T. J. (2014). Global and time-resolved monitoring of crop photosynthesis with chlorophyll fluorescence. *Proceedings of the National Academy of Sciences*, 111, E1327–E1333. https://doi.org/10.1073/pnas.1320008111
- Gutman, G., & Ignatov, A. (1998). The derivation of the green vegetation fraction from NOAA/AVHRR for use in numerical weather prediction models. *International Journal of Remote Sensing*, 19, 1533–1543. https://doi.org/10.1080/014311698215333
- Hatfield, J. L., Asrar, G., & Kanemasu, E. T. (1984). Intercepted photosynthetically active radiation estimated by spectral reflectance. *Remote sensing of Environment*, 14, 65–75. https://doi.org/10.1016/0034-4257(84)90008-7
- Hernández-Clemente, R., North, P. R. J., Hornero, A., & Zarco-Tejada, P. J. (2017). Assessing the effects of forest health on sun-induced chlorophyll fluorescence using the FluorFLIGHT 3-D radiative transfer model to account for forest structure. Remote Sensing of Environment, 193, 165–179. https://doi.org/10.1016/j.rse.2017.02.012
- Hoge, F. E., Swift, R. N., & Yungel, J. K. (1983). Feasibility of airborne detection of laser-induced fluorescence emissions from green terrestrial plants. *Applied Optics*, 22(19), 2991–3000. https://doi.org/10. 1364/AO.22.002991
- Hubbard, R. M., Yoder, B. J., & Ryan, M. G. (1999). Evidence that hydraulic conductance limits photosynthesis in old Pinus ponderosa trees. Tree Physiology, 19, 165–172. https://doi.org/10.1093/treephys/19.3.
- Jiménez-Muñoz, J. C., Sobrino, J. A., Guanter, L., Moreno, J., Plaza, A., & Martínez, P. (2005). Fractional vegetation cover estimation from PROBA/CHRIS data: Methods, analysis of angular effects and application to the land surface emissivity. 3rd ESA CHRIS/Proba Workshop 21–23 March, ESRIN (Frascati, Italy).
- Joiner, J., Yoshida, Y., Guanter, L., & Middleton, E. M. (2016). New methods for retrieval of chlorophyll red fluorescence from hyper-spectral satellite instruments: Simulations and application to GOME-2 and SCIAMACHY. Atmospheric Measurement Techniques, 9, 3939. https://doi.org/10.5194/amt-9-3939-2016

- Joiner, J., Yoshida, Y., Vasilkov, A. P., Schaefer, K., Jung, M., Guanter, L., ... Belelli Marchesini, L. (2014). The seasonal cycle of satellite chlorophyll fluorescence observations and its relationship to vegetation phenology and ecosystem atmosphere carbon exchange. *Remote Sensing of Environment*, 152, 375–391. https://doi.org/10.1016/j.rse. 2014.06.022
- Knyazikhin, Y., Schull, M. A., Stenberg, P., Mottus, M., Rautiainen, M., Yang, Y., ... Myneni, R. B. (2012). Hyperspectral remote sensing of foliar nitrogen content. Proceedings of the National Academy of Sciences of the United States of America, 110(3), E185–E192.
- Koffi, E. N., Rayner, P. J., Norton, A. J., Frankenberg, C., & Scholze, M. (2015). Investigating the usefulness of satellite-derived fluorescence data in inferring gross primary productivity within the carbon cycle data assimilation system. *Biogeosciences*, 12(13), 4067–4084. https://doi.org/10.5194/bg-12-4067-2015
- Larcher, W. (1969). The effect of environmental and physiological variables in the carbon dioxide exchange of trees. *Photosynthetica*, 3, 16.
- Latifovic, R., & Olthof, J. (2004). Accuracy assessment using sub-pixel fraction error matrices of global land cover products derived from satellite data. Remote Sensing of Environment, 90, 153–165. https://d oi.org/10.1016/j.rse.2003.11.016
- Lee, J. E., Frankenberg, C., van der Tol, C., Berry, J. A., Guanter, L., Boyce, C. K., ... Saatchi, S. (2013). Forest productivity and water stress in Amazonia: Observations from GOSAT chlorophyll fluorescence. *Proceedings of the Royal Society B: Biological Sciences*, 280 (1761), 20130171. https://doi.org/10.1098/rspb.2013.0171
- Linkosalo, T., Heikkinen, J., Pulkkinen, P., & Mäkipää, R. (2014). Fluorescence measurements show stronger cold inhibition of photosynthetic light reactions in Scots pine compared to Norway spruce as well as during spring compared to autumn. *Frontiers in Plant Science*, *5*, 264.
- Liu, L., Guan, L., & Liu, X. (2017). Directly estimating diurnal changes in GPP for C3 and C4 crops using far-red sun-induced chlorophyll fluorescence. Agricultural and Forest Meteorology, 232, 1–9. https://doi. org/10.1016/j.agrformet.2016.06.014
- Louis, J. A., Ounis, J. M., Ducruet, S., Evain, T., Laurila, T., Thum, M., ... Moya, I. (2005). Remote sensing of sunlight-induced chlorophyll fluorescence and reflectance of scots pine in the boreal forest during spring recovery. *Remote Sensing of Environment*, *96*(1), 37–48. https://doi.org/10.1016/j.rse.2005.01.013
- Maier, C. A., Johnsen, K., Butnor, J., Kress, L. W., & Anderson, P. H. (2002). Branch growth and gas exchange in 13-year-old loblolly pine (*Pinus taeda*) trees in response to elevated carbon dioxide concentration and fertilization. *Tree Physiology*, 22, 1093–1106. https://doi.org/ 10.1093/treephys/22.15-16.1093
- Malenovský, Z., Homolová, L., Zurita-Milla, R., Lukeš, P., Kaplan, V., Hanuš, J., ... Schaepman, M. E. (2013). Retrieval of spruce leaf chlorophyll content from airborne image data using continuum removal and radiative transfer. *Remote Sensing of Environment*, 131, 85–102. https://doi.org/10.1016/j.rse.2012.12.015
- Meinzer, F. C., Lachenbruch, B., & Dawson, T. E.. (2011). Size- and agerelated changes in tree structure and function. Berlin: Springer Science & Business Media, 514 p. https://doi.org/10.1007/978-94-007-1242-3
- Meroni, M., & Colombo, R. (2006). Leaf level detection of solar induced chlorophyll fluorescence by means of a subnanometer resolution spectroradiometer. *Remote Sensing of Environment*, 103(4), 438–448. https://doi.org/10.1016/j.rse.2006.03.016
- Meroni, M., Rossini, M., Guanter, L., Alonso, L., Rascher, U., Colombo, R., & Moreno, J. (2009). Remote sensing of solar-induced chlorophyll fluorescence: Review of methods and applications. Remote Sensing of Environment, 113(10), 2037–2051. https://doi.org/10.1016/j.rse. 2009.05.003
- Meroni, M., Rossini, M., Picchi, V., Panigada, C., Cogliati, S., Nali, C., & Colombo, R. (2008). Assessing steady-state fluorescence and PRI from hyperspectral proximal sensing as early indicators of plant

- stress: The case of ozone exposure. *Sensors*, *8*(3), 1740–1754. https://doi.org/10.3390/s8031740
- Middleton, E. M., Cheng, Y. B., Campbell, P. E., Huemmrich, K. F., Corp, L. A., Bernardes, S., ... Russ, A. L. (2015). Multi-angle hyperspectral observations with SIF and PRI to detect plant stress & GPP in a cornfield. Proceedings 9th EARSeL SIG Workshop on Imaging Spectroscopy, CD-ROM, Luxembourg City, Luxembourg, April 2015, 10 pp.
- Middleton, E. M., Huemmrich, K. F., Cheng, Y. B., & Margolis, H. A. (2012). Spectral bio-indicators of photosynthetic efficiency and vegetation stress. In P. S. Thenkabail, J. G. Lyon & A. Huete (Eds.), Hyperspectral remote sensing of vegetation (pp. 265–280). Abingdon-on-Thames, UK: Taylor & Francis.
- Middleton, E. M., Rascher, U., Corp, L. A., Huemmrich, F. K., Cook, B. D., Noormets, A., ... Bianchi, R. (2017). The 2013 FLEX-US airborne campaign at the parker tract loblolly pine plantation in North Carolina, USA. Remote Sensing, 9(6), 612. https://doi.org/10.3390/ rs9060612
- Moya, I., Camenenb, L., Evain, S., Goulas, Y., Cerovic, Z. G., Latouche, G., ... Ounis, A. (2004). A new instrument for passive remote sensing: 1. Measurements of sunlight-induced chlorophyll fluorescence. *Remote Sensing of Environment*, 91, 186–197. https://doi.org/10.1016/j.rse. 2004.02.012
- Moya, I., Daumard, F., Moise, N., Ounis, A., & Goulas, Y. (2006). First airborne multiwavelength passive chlorophyll fluorescence measurements over La Mancha (Spain) fields, 2nd International Symposium on Recent Advances in Quantitative Remote Sensing: RAQRS'II, 25–29th September, Torrent (Valencia)-Spain.
- Myneni, R. B., Hoffman, S., Knyazikhin, Y., Privette, J. L., Glassy, J., Tian, Y., ... Running, S. W. (2002). Global products of vegetation leaf area and fraction absorbed PAR from year one of MODIS data. *Remote Sensing of Environment*, 83, 214–231. https://doi.org/10.1016/S0034-4257(02)00074-3
- Myneni, R. B., & Williams, D. L. (1994). On the relationship between FAPAR and NDVI. Remote Sensing of Environment, 49(3), 200–211. https://doi.org/10.1016/0034-4257(94)90016-7
- Noormets, A., Gavazzi, M., McNulty, S. G., Domec, J. C., Sun, G., King, J. S., & Chen, J. (2010). Response of carbon fluxes to drought in a coastal plain loblolly pine forest. *Global Change Biology*, 16, 272–287. https://doi.org/10.1111/(ISSN)1365-2486
- North, P. R. J. (2002). Estimation of fAPAR, LAI, and vegetation fractional cover from ATSR-2 imagery. *Remote Sensing of Environment*, 80(1), 114–121. https://doi.org/10.1016/S0034-4257(01)00292-9
- Novick, K., Oren, R., Stoy, P., Juang, J. Y., Siqueira, M., & Katul, G. (2009). The relationship between reference canopy conductance and simplified hydraulic architecture. Advances in Water Resources, 32, 09–819.
- Olioso, A., Méthy, M., & Lacaze, B. (1992). Simulation of canopy fluorescence as a function of canopy structure and leaf fluorescence. *Remote Sensing of Environment*, 41, 239–247. https://doi.org/10.1016/0034-4257(92)90081-T
- Olthof, I., & Fraser, R. H. (2007). Mapping northern land cover fractions using Landsat ETM+. *Remote Sensing of Environment*, 107, 496–509. https://doi.org/10.1016/j.rse.2006.10.009
- Oren, R., Hsieh, C. I., Stoy, P., Albertson, J., McCarthy, H. R., Harrell, P., & Katul, G. G. (2006). Estimating the uncertainty in annual net ecosystem carbon exchange: Spatial variation in turbulent fluxes and sampling errors in eddy-covariance measurements. *Global Change Biology*, 12, 883–896. https://doi.org/10.1111/j.1365-2486.2006. 01131.x
- Pickett-Heaps, C. A., Canadell, J. G., Briggs, P. R., Gobron, N., Haverd, V., Paget, M. J., ... Raupach, M. R. (2014). Evaluation of six satellitederived Fraction of Absorbed Photosynthetic Active Radiation (FAPAR) products across the Australian continent. *Remote Sensing of Environment*, 140, 241–256. https://doi.org/10.1016/j.rse.2013.08. 037

- Porcar-Castell, A., Tyystjarvi, E., Atherton, J., van der Tol, C., Flexas, J., Pfuendel, E. E., ... Berry, J. A. (2014). Linking chlorophyll a fluorescence to photosynthesis for remote sensing applications: Mechanisms and challenges. *Journal of Experimental Botany*, 65(15), 4065–4095. https://doi.org/10.1093/jxb/eru191
- Quantum GIS Development Team (2016). Quantum GIS Geographic Information System. Open Source Geospatial Foundation Project, http://qgis.osgeo.org.
- Rascher, U., Agati, G., Alonso, L., Cecchi, G., Champagne, S., Colombo, R., ... Zaldei, A. (2009). CEFLES2: The remote sensing component to quantify photosynthetic efficiency from the leaf to the region by measuring sun-induced fluorescence in the oxygen absorption bands. *Biogeosciences*, 6, 1181–1198. https://doi.org/10.5194/bg-6-1181-2009
- Rascher, U., Alonso, L., Burkart, A., Cilia, C., Cogliati, S., Colombo, R., . . . Zemek, F. (2015). Sun-induced fluorescence a new probe of photosynthesis: First maps from the imaging spectrometer HyPlant. Global Change Biology, 21(12), 4673–4684. https://doi.org/10.1111/gcb. 13017
- Rascher, U., Bobich, E. G., Lin, G. H., Walter, A., Morris, T., Naumann, M., ... Berry, J. A. (2004). Functional diversity of photosynthesis during drought in a model tropical rainforest—the contributions of leaf area, photosynthetic electron transport and stomatal conductance to reduction in net ecosystem carbon exchange. *Plant, Cell & Environment*, 27, 1239–1256. https://doi.org/10.1111/j.1365-3040.2004. 01231.x
- Reinhardt, K., Johnson, D. M. J. M., & Smith, W. K. S. K. (2009). Ageclass differences in shoot photosynthesis and water relations of Fraser fir (Abies fraseri), southern Appalachian Mountains, USA. Canadian Journal of Forest Research, 39(1), 193–197. https://doi.org/10. 1139/X08-163
- Rossini, M., Meroni, M., Celesti, M., Cogliati, S., Julitta, T., Panigada, C., ... Colombo, R. (2016). Analysis of red and far-red sun-induced chlorophyll fluorescence and their ratio in different canopies based on observed and modeled data. *Remote Sensing*, 8(5), 412. https://doi.org/10.3390/rs8050412
- Rossini, M., Meroni, M., Migliavacca, M., Manca, G., Cogliati, S., Busetto, L., ... Colombo, R. (2010). High resolution field spectroscopy measurements for estimating gross ecosystem production in a rice field. Agricultural and Forest Meteorology, 150(9), 1283–1296. https://doi. org/10.1016/j.agrformet.2010.05.011
- Rossini, M., Nedbal, L., Guanter, L., Ač, A., Alonso, L., Burkart, A., ... Rascher, U. (2015). Red and far red Sun-induced chlorophyll fluorescence as a measure of plant photosynthesis. *Geophysical Research Letters*, 42, 1632–1639. https://doi.org/10.1002/2014GL062943
- Rundel, P. W., & Yoder, B. J. (1998). Ecophysiology of pinus. In D. M. Richardson (Ed.), Ecology and biogeography of pinus (pp. 296–323). Cambridge, UK: Cambridge University Press.
- Running, S. W., & Gower, S. T. (1991). FOREST-BGC, a general model of forest ecosystem processes for regional applications, II. Dynamic carbon allocation and nitrogen budgets. *Tree Physiology*, 9, 147–160. https://doi.org/10.1093/treephys/9.1-2.147
- Ryan, M. G., Binkley, D., & Fownes, J. H. (1996). Age-related decline in forest productivity: Pattern and process. Advances in Ecological Research, 27, 213–262.
- Ryan, M. G., Binkley, D., Fownes, J. H., Giardina, C. P., & Senock, R. S. (2004). An experimental test of the causes of forest growth decline with stand age. *Ecological Monographs*, 74(3), 393–414. https://doi.org/10.1890/03-4037
- Ryan, M. G., Phillips, N., & Bond, B. J. (2006). The hydraulic limitation hypothesis revisited. *Plant, Cell and Environment*, 29, 367–381. https://doi.org/10.1111/j.1365-3040.2005.01478.x
- Ryan, M. J., & Yoder, B. J. (1997). Hydraulic limits to tree height and tree growth. *BioScience*, 47, 235–242. https://doi.org/10.2307/1313077
- Shirke, P. A. (2001). Leaf photosynthesis, dark respiration and fluorescence as influenced by leaf age in an evergreen tree, *Prosopis*

- Juliflora. Photosynthetica, 39(2), 305–311. https://doi.org/10.1023/A: 1013761410734
- Sun, Y., Fu, R., Dickinson, R., Joiner, J., Frankenberg, C., Gu, L., ... Fernando, N. (2015). Drought onset mechanisms revealed by satellite solar-induced chlorophyll fluorescence: Insights from two contrasting extreme events. *Journal of Geophysical Research*: Biogeosciences, 120, 2427–2440.
- Tasissa, G., & Burkhart, H. E. (1998). Juvenile-mature wood demarcation in loblolly pine trees. *Wood and Fiber Science*, 30(2), 119–127.
- van der Tol, C., Rossini, M., Cogliati, S., Verhoef, W., Colombo, R., Rascher, U., & Mohammed, G. (2016). A model and measurement comparison of diurnal cycles of sun-induced chlorophyll fuorescence of crops. *Remote Sensing of Environment*, 186, 663–677.
- van der Tol, C., Verhoef, W., Timmermans, J., Verhoef, A., & Su, Z. (2009). An integrated model of soil - canopy spectral radiances, photosynthesis, fluorescence, temperature and energy balance. *Biogeosciences*, 6, 3109–3129.
- Van Wittenberghe, S., Alonso, L., Verrelst, J., Hermans, I., Delegido, J., Veroustraete, F., . . . Samson, R. (2013). Upward and downward solar-induced chlorophyll fluorescence yield indices of four tree species as indicators of traffic pollution in Valencia. *Environmental Pollution*, 173, 29–37. https://doi.org/10.1016/j.envpol.2012.10.003
- Verhoef, W., & Bach, H. (2007). Coupled soil leaf canopy and atmosphere radiative transfer modeling to simulate hyperspectral multi angular surface reflectance and TOA radiance data. *Remote Sensing of Environment*, 109(2), 166–182. https://doi.org/10.1016/j.rse.2006.12.013
- Verrelst, J., Rivera, J. P., van der Tol, C., Magnani, F., Mohammed, G., & Moreno, J. (2015). Global sensitivity analysis of the SCOPE model: What drives simulated canopy-leaving sun-induced fluorescence? Remote Sensing of Environment, 166, 8–21. https://doi.org/10.1016/j. rse 2015.06.002
- Verrelst, J., van der Tol, C., Magnani, F., Sabater, N., Rivera, J. P., Mohammed, G., & Moreno, J. (2016). Evaluating the predictive power of sun-induced chlorophyll fluorescence to estimate net photosynthesis of vegetation canopies: A SCOPE modeling study. Remote Sensing of Environment, 176, 139–151. https://doi.org/10.1016/j.rse.2016.01. 018
- Walter-Shea, E. A., Privette, J., Cornell, D., Mesarch, M. A., & Hays, C. J. (1997). Relations between directional spectral vegetation indices and leaf area and absorbed radiation in alfalfa. Remote Sensing of Environment, 61, 162–177. https://doi.org/10.1016/S0034-4257(96)00250-7
- Widlowski, J. L. (2010). On the bias of instantaneous FAPAR estimates in open-canopy forests. *Agricultural and Forest Meteorology*, 150, 1501–1522. https://doi.org/10.1016/j.agrformet.2010.07.011
- Wieneke, S., Ahrends, H., Damm, A., Pinto, F., Stadler, A., Rossini, M., & Rascher, U. (2016). Airborne based spectroscopy of red and far-red sun-induced chlorophyll fluorescence: Implications for improved estimates of gross primary productivity. Remote Sensing of Environment, 184, 654–667. https://doi.org/10.1016/j.rse.2016.07.025

- Yoder, B. J., Ryan, M. G., Waring, R. H., Schoettle, A. W., & Kaufmann, M. R. (1994). Evidence of reduced photosynthetic rates in old trees. Forest Science, 40, 513–527.
- Zarco-Tejada, P. J., González-Dugo, V., & Berni, J. A. J. (2012). Fluorescence, temperature and narrow-band indices acquired from a UAV platform for water stress detection using a micro-hyperspectral imager and a thermal camera. *Remote Sensing of Environment*, 117, 322–337. https://doi.org/10.1016/j.rse.2011.10.007
- Zarco-Tejada, P. J., González-Dugo, M. V., & Fereres, E. (2016). Seasonal stability of chlorophyll fluorescence quantified from airborne hyperspectral imagery as an indicator of net photosynthesis in the context of precision agriculture. *Remote Sensing of Environment*, 179, 89–103. https://doi.org/10.1016/j.rse.2016.03.024
- Zarco-Tejada, P. J., Miller, J. R., Harron, J., Hu, B., Noland, T. L., Goel, N., ... Sampson, P. (2004). Needle chlorophyll content estimation through model inversion using hyperspectral data from boreal conifer forest canopies. *Remote Sensing of Environment*, 89, 189–199. https://doi.org/10.1016/j.rse.2002.06.002
- Zarco-Tejada, P. J., Suarez, L., & Gonzalez-Dugo, V. (2013). Spatial resolution effects on chlorophyll fluorescence retrieval in a heterogeneous canopy using hyperspectral imagery and radiative transfer simulation. *IEEE Geoscience and Remote Sensing Letters*, 10(4), 937–941. https://doi.org/10.1109/LGRS.2013.2252877
- Zeide, B. (1993). Analysis of growth equations. Forest Science, 39(3), 594–616
- Zhang, Y., Guanter, L., Berry, J. A., Joiner, J., van der Tol, C., Huete, A., ... Kohler, P. (2014). Estimation of vegetation photosynthetic capacity from space-based measurements of chlorophyll fluorescence for terrestrial biosphere models. *Global Change Biology*, 20(12), 3727–3742. https://doi.org/10.1111/gcb.12664
- Zhang, Q., Middleton, E. M., Cheng, Y. B., Huemmrich, K. F., Cook, B. D., Corp, L. A., . . . Yao, T. (2016). Integrating Chlorophyll fapar and nadir photochemical reflectance index from EO-1/hyperion to predict cornfield daily gross primary production. *Remote Sensing of Environment*, 186, 311–321. https://doi.org/10.1016/j.rse.2016.08.026
- Zhao, F., Dai, X., Verhoef, W., Guo, Y., van der Tol, C., Li, Y., & Huang, Y. (2016). FluorWPS: A Monte Carlo ray-tracing model to compute sun-induced chlorophyll fluorescence of three-dimensional canopy. Remote Sensing of Environment, 187, 385–399. https://doi.org/10.1016/j.rse.2016.10.036

How to cite this article: Colombo R, Celesti M, Bianchi R, et al. Variability of sun-induced chlorophyll fluorescence according to stand age-related processes in a managed loblolly pine forest. *Glob Change Biol*. 2018;24:2980–2996. https://doi.org/10.1111/gcb.14097